1. Report No.	2. Government Accession No.	3. Recipient's Catalog No.
FHWA/TX-09/0-6037-1		

4. Title and Subtitle	5. Report Date
SUBBASE AND SUBGRADE PERFORMANCE INVESTIGATION FOR CONCRETE PAVEMENT	January 2009 Published: May 2009
	6. Performing Organization Code
7. Author(s)	8. Performing Organization Report No.
Youn su Jung, Dan G. Zollinger, Moon Won, and Andrew J. Wimsatt	Report 0-6037-1
9. Performing Organization Name and Address Texas Transportation Institute The Texas A&M University System College Station, Texas 77843-3135	10. Work Unit No. (TRAIS)
	11. Contract or Grant No. Project 0-6037
12. Sponsoring Agency Name and Address Texas Department of Transportation Research and Technology Implementation Office P.O. Box 5080 Austin, Texas 78763-5080	13. Type of Report and Period Covered Technical Report: September 2007-September 2008
	14. Sponsoring Agency Code

15. Supplementary Notes

Project performed in cooperation with the Texas Department of Transportation and the Federal Highway Administration.
Project Title: Alternatives to Asphalt Concrete Pavement Subbases for Concrete Pavement
URL: http://tti.tamu.edu/documents/0-6037-1.pdf

16. Abstract

Recently, TxDOT has become increasingly aware of the rising cost associated with the use of asphalt concrete bond breakers to meet the FHWA requirement of using a permanently stabilized, nonerodable subbase layer below the concrete slab. The main issue associated with this research is if cheaper alternatives are available for subbase construction. Subbase layers have certain functions that need to be fulfilled (one of them being constructability) in order to assure adequate pavement performance. One key aspect is resistance to erosion, and assessment of each of these functions relative to different alternatives is key to understanding the capability of different alternatives to perform adequately. In this respect, this project is to examine the design assumptions associated with each alternative and provide recommendations accordingly to include test methods and material specifications.

This report describes some of the work accomplished summarizing data on subbase performance and testing relative to concrete pavement subbase and subgrade erosion. Findings from investigations are discussed to identify factors associated with erosion in the field based on various analysis methods such as load transfer efficiency (LTE), effective thickness, and ground penetrating radar (GPR). An approach to mechanistically consider the erosion process is introduced and review of current design procedures was also conducted as to how they address erosion. This review was extended to address erosion models included in the literature in terms of the relationship between measurable material properties and performance. Moreover, previous and current laboratory test methods for erosion testing are summarized and the test results of selected alternative subbase materials are discussed. Finally, the relation between k-value and slab behavior is discussed.

17. Key Words	18. Distribution Statement
Subbase Material, Erosion, Field Performance, Concrete Pavement, k-value, GPR, FWD, DCP, Static Plate Load Test	No restrictions. This document is available to the public through NTIS: National Technical Information Service Springfield, Virginia 22161 http://www.ntis.gov

19. Security Classif.(of this report)	20. Security Classif.(of this page)	21. No. of Pages	22. Price
Unclassified	Unclassified	112	

SUBBASE AND SUBGRADE PERFORMANCE INVESTIGATION FOR CONCRETE PAVEMENT

by

Youn su Jung
Graduate Research Assistant
Texas Transportation Institute

Dan G. Zollinger
Program Manager
Texas Transportation Institute

Moon Won
Research Associate Professor
Center for Transportation Research

and

Andrew J. Wimsatt
Division Head
Texas Transportation Institute

Report 0-6037-1
Project 0-6037
Project Title: Alternatives to Asphalt Concrete Pavement Subbases for Concrete Pavement

Performed in cooperation with the
Texas Department of Transportation
and the
Federal Highway Administration

January 2009
Published: May 2009

TEXAS TRANSPORTATION INSTITUTE
The Texas A&M University System
College Station, Texas 77843-3135

DISCLAIMER

The contents of this report reflect the views of the authors, who are responsible for the facts and the accuracy of the data presented herein. The contents do not necessarily reflect the official view or policies of the Federal Highway Administration (FHWA) or the Texas Department of Transportation (TxDOT). This report does not constitute a standard, specification, or regulation. Its contents are not intended for construction, bidding, or permit purposes. The use of names of specific products or manufacturers listed herein does not imply endorsement of those products or manufacturers. The engineer in charge of the project was Andrew J. Wimsatt, Texas P.E., #72270.

ACKNOWLEDGMENTS

This project was conducted in cooperation with TxDOT and FHWA. The authors wish to express their appreciation of the personnel of the Federal Highway Administration and the Texas Department of Transportation for their support throughout this project, as well as of the project coordinator, David Head (El Paso District Director of Construction) the project director, Ralph Browne (Fort Worth District North Tarrant County Area Engineer), and members of the Project Monitoring Committee, Buddy (Jere) Williams, Darrell Anglin, Doug Beer, Eric Ingamells, Hua Chen, and David Head.

TABLE OF CONTENTS

Page

TABLE OF CONTENTS

Page

TABLE OF CONTENTS

Page

LIST OF FIGURES

Page

LIST OF FIGURES

Page

LIST OF FIGURES

Page

LIST OF TABLES

Page

Chapter 1
INTRODUCTION

One of the most evolving elements of concrete pavement design in the last 40 years has been the type and nature of the materials used in the subbase layer immediately below a concrete pavement. Over this period of time, subbases have consisted of both dense and open-graded unbound materials, different varieties of cement-treated bases (both asphalt and portland), lean concrete bases, and then back to cement-treated bases (CTB) but with an asphalt cement (AC) bond breaker layer. Lean concrete subbases, although highly erosion resistant, have been far too stiff for conventional jointed concrete pavements and less stiff CTBs have not been erosion resistant enough unless combined with an interlayer. Nonetheless, some level of stabilization seems to be the most popular trend as of late, but subbases with high friction properties have been found to be problematic relative to the formation of well-distributed cracking patterns.

Since a primary focus of this research is to identify alternative materials for subbase layer applications, it is useful to consider the purposes and functions of a concrete pavement subbase layer:

1. To provide a stable construction platform,
2. To provide uniform slab support,
3. To prevent erosion of the pavement support,
4. To facilitate drainage,
5. To provide increased slab support, and
6. To provide a gradual vertical transition in layer moduli.

This list is perhaps not all inclusive but certainly covers the major functions of a subbase layer under a concrete pavement system. Even if a subbase fulfills no other purpose other than to facilitate construction of the pavement system it is perhaps, justification enough to be included in the pavement design since not all design scenarios require that a subbase layer be structurally included, such as for low-volume road designs with subgrades in certain strength ranges. The need for a subbase is mainly driven by the

design traffic and load level. Consequently, the natural default function of a subbase layer beyond any relevant construction issues is to provide uniform support—where failure to do so will invalidate any pretense of providing a long-lasting pavement section.

The role of uniform support cannot be overstated in the performance of long-lasting concrete pavement systems; good performing concrete pavements can co-exist with a wide range of support strength, but variation from the slab center to the edge or corner area or differences in support between segments of continuously reinforced concrete (CRC) pavement, for instance, cannot be tolerated to any great extent (Figure 1), which is why erosion is and has been a key factor in performance. Loss of support along pavement shoulder and longitudinal joint areas has been identified as the key factors in the development of punchout distress in CRC pavement systems. These play a prominent role in the punchout process since they directly impact shear stress on the face of transverse cracks where aggregate interlock occurs to transfer load between adjacent slab segments. Increase in shear stress will increase the rate of aggregate wear out that ultimately leads to lower load transfer and increased lateral bending stress. However, as long as support conditions can be maintained and wear out of aggregate interlock minimized, bending stresses in CRC pavement systems will be relatively small, which results, for all practical purposes, in an infinitely long fatigue life. Otherwise, it is critical in the design stage to account for less than full support conditions in slab areas where erosion has a potential of occurring.

Erosion potential is greatest where upward curling and warping along edge and corner areas debond the slab from the subbase enabling the slab to "pump" any water that may be trapped under applied wheel loads back and forth across the slab/subbase interface. This action, combined with the viscous nature of water, creates a shearing stress that carries eroded subbase material, further disrupting the continuity of the slab support. In this sense, one could argue that the third function is really a subset of the second function since erosion creates a nonuniform support condition that often leads to faulting in jointed pavements and punchouts in CRC pavements.

Figure 1. Effects of Erosion on CRC Pavement Performance.

Another interesting function of a subbase layer is to provide drainability which may have different meanings depending on whether moisture is able to permeate the subbase layer or be drawn into it through capillary action. Most concrete pavement types will manifest some evidence of pumping if (1) water is present along the interface between the slab and the subbase or subgrade and (2) the subbase or subgrade is susceptible to erosion. Any means to remove or to minimize the presence of moisture on the interface is considered effective drainage; however, the means to do that may vary depending on the drainability of the subgrade materials.

Subbase materials stiff enough to resist erosive forces under the action of pumping may not require drainage within the material but only enough unobstructed cross slope to allow the removal of water from the interface to be effective. Unfortunately, most CTB subbases are not sufficiently erosive resistant or permeable to allow for a timely removal of water to avoid erosion damage. The use of an asphalt interlayer has certainly improved the erosion resistance of CTB but the main reason for using such materials has been to reduce the frictional resistance between the slab and the subbase to ensure proper development of the crack pattern in CRC pavements. Clearly, the asphalt interlayer has served two purposes as far a CRC pavement design and performance.

The use of open-graded drainable stabilized layers has been a consideration but interlocking between the two layers can be cause of concern. Also, drainable stabilized

layers have had constructability and stability issues. Dallas District personnel changed the subbase on the North Central Expressway (US 75) project from an open-graded asphalt stabilized subbase to a regular dense-graded base because the open-graded base was difficult to construct and was unstable under construction traffic.

Functions 5 (to provide increased slab support) and 6 (to provide a gradual vertical transition in layer moduli) may tend to counter the effects of each other but nonetheless refer to some key aspects of subbase requirements. Subbase layers certainly can add structural capacity to a concrete pavement but the contribution in this regard is generally small in light of the inherent load spreading capability of the slab. Consequently, this function is not an absolute necessity and can be sacrificed to some extent. Perhaps a more important feature is provision of a gradual change in layer stiffness from the slab to the top of the subgrade layer. Abrupt changes in this regard can lead to undesirable load concentrations along the corners and pavement edges, enhancing the effect of poor support conditions over time and loading cycles. Stiff subbases also tend to magnify the environmentally induced load stresses in the slab and shorten the fatigue life of the pavement system. Again, the use of an AC interlayer helped reduce these types of stresses and prolong the fatigue life of the slab by reducing the curling and warping-related stresses.

CHAPTER 2
FIELD INVESTIGATIONS

The objectives of the field investigation were to identify the factors associated with the erosion process. Sample sections were identified and investigated using a number of techniques including visual survey, nondestructive testing using falling weight deflectometer (FWD), and the ground penetrating radar (GPR) as well as dynamic cone penetrometer (DCP) and coring.

Table 1 shows the performance of non-asphalt treated subbase of certain pavement sections in Texas. Generally, untreated flexible base and lime-treated subgrade have not performed well under both CRC and jointed concrete (JC) pavement. These sections have pumped fines through the matrix diplacing the fines causing voiding of the subbase layer. However, a portion constructed in the 1950s over a seal-coated flexible base has been performing well; this section was constructed on elevated ground facilitating good drainage and unsaturated conditions in the subgrade. The presence of the seal coat may also help to reduce moisture intrusion into the base and the friction between a slab and a flex base would be minimal.

Most cement stabilized bases (CSB) in Texas placed without a bond breaker have performed well under all types of concrete pavements and traffic levels since CSB is highly resistant to erosion. However, sections statewide with weakly CSBs built during 1950s and 1960s have shown premature failures possibly due to the low cement content of these bases. Detailed evaluations of selected sections are subsequently discussed with test results and photos

.

Table 1. Subbase Type and Performance of Highways in Texas.

Poorly Performing Subbases	Well Performing Subbases
Statewide – 8 in CRC pavement over weak cement stabilized bases (CSB) (1950s-1960s)	**IH 30 in Fort Worth** – 8 in CRC pavement over seal coat and flexible base, built in late 1950s (overlaid with 2 in ACP, still in place)
IH 35E near Waxahachie – 8 in CRC pavement over flexible base, built in the 1960s	**IH 10 in El Paso** – 8 in CRC pavement built directly over CSB
US 75 near Sherman – 10 in CPCD over flexible base, built in the early 1980s	**IH 10 in Houston** – 8 in CRC pavement over CSB
IH 35W N. of Fort Worth – 8 in CRC pavement over lime-treated subgrade, built in the 1960s	**Beaumont District** – Concrete Pavement Contraction Design (CPCD) over CSB
Various roadways in Atlanta and Childress – 13 in CPCD (no dowels) over natural subgrade (usually sandy)	**IH 45 in Houston** – 8 in Jointed Reinforced Concrete Pavement (JRCP) over Oyster Shell Base (1945)

US 75—SHERMAN DISTRICT

Sections of a 10 in JC that was jointed at 15 ft intervals and built in 1983 were sampled to investigate the 6 in unbound aggregate base and natural weathered soil subgrade it was placed on. This JC pavement had been faulted in areas since the early 1990s because of severely deteriorated joint seals and moisture intrusion taking place over the years weakening the subgrade and contaminating the base. Overall, the drainage condition was visually poor since there was a significant amount of standing water in the ditches alongside the sampled sections. Table 2 shows a visual summary of the surveyed conditions.

Table 2. JC Pavement Condition Survey of US 75 (Poor Performing Section).

No.	Checklist	Notes
1	Pavement age (yr)	24 yr, 15 ft joint spacing
2	Aggregate type (hard or soft)	Soft — limestone
3	Year of recent pavement distress survey (yr)	N/A
4	Year of recent pavement deflection survey (yr)	N/A
5	Joint sealant age (yr)	N/A
6	Sealant damage of transverse joint (%)	50%
7	Sealant damage of longitudinal joint (%)	80%
8	Sealant damage of sealed crack (%)	No seal on crack
9	Trapped surface water in depressed area	No
10	Standing water or slab staining	Yes — shoulder
11	Pumping with or without staining	Positive
12	Bump (stable or unstable; depth, in)	No
13	Settlement (stable or unstable; depth, in)	Repaired
14	Joint spall (width, depth, % of joint spall > 2 in)	3 in, 2 in, 20%
15	Crack spall (width, depth, % of crack spall > 2 in)	2 in, 1 in, 10%
16	Deep spall (depth, in)	No
17	Patching (number/mi)	35
18	Faulting (depth, in)	Repaired
19	Transverse crack (width, number/slab)	0.05 in, 2/10
20	Longitudinal crack (width, number/slab)	0.04 in, 1/10
21	Shoulder separation (width, in)	1/4 in joint well damage
22	Corner break (spall width, fault depth, % of slab)	12 in × 10 in, 5%
23	Reflection crack in asphalt concrete overlay (ACOL)	N/A

The sampled data suggested the project could be divided into four sections as noted in Figure 2: (1) good performing areas (with no cracks), (2) poor performing condition areas (with more than one crack), (3) areas with patches more than 5 years old, and (4) newly patched slabs (approximately 1 to 2 years old). The good performing and patched areas showed no distress but the joint sealing appeared to be well maintained. Poorly performing sections typically showed significant joint seal deterioration particularly along the joints between the lanes and the shoulder, which apparently lead to significant base and subgrade erosion.

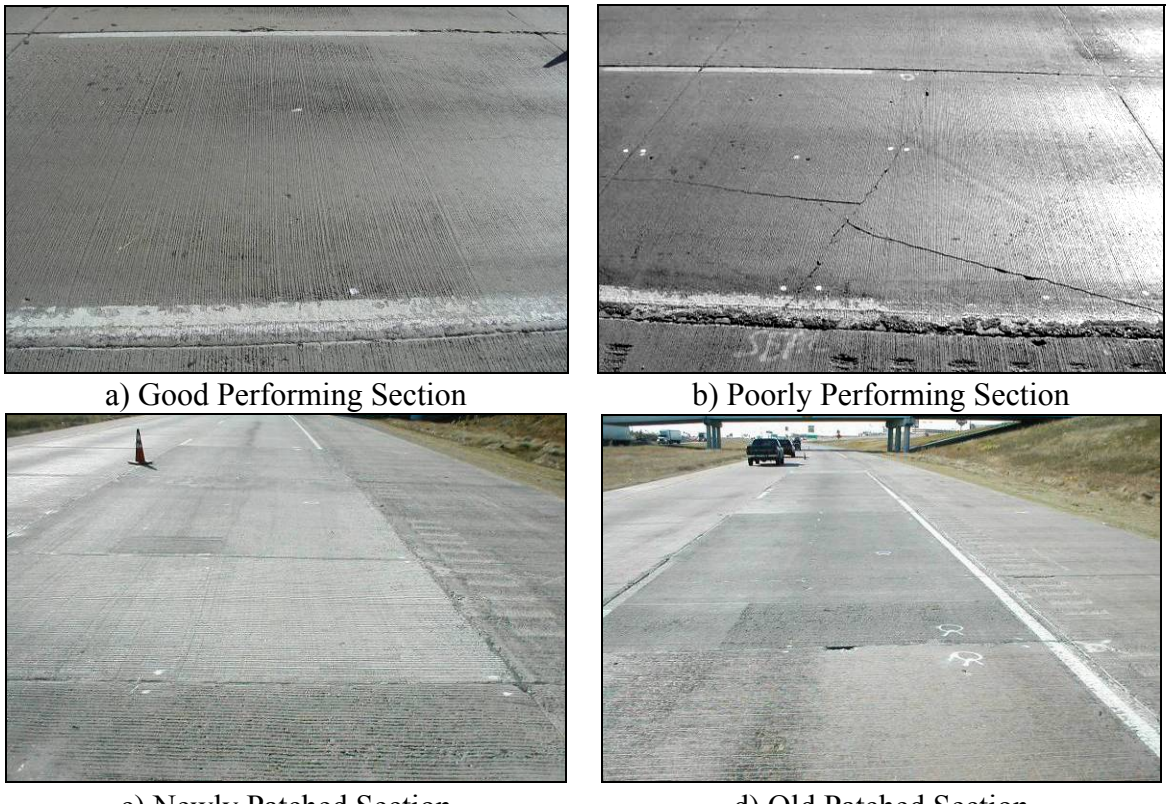

a) Good Performing Section b) Poorly Performing Section

c) Newly Patched Section d) Old Patched Section

Figure 2. Test Sections on US 75.

Figure 3 shows a deteriorating pavement condition apparently due to softening subgrade conditions caused by intrusion of water. Damaged joint seals (especially at shoulder joints) often allow for the penetration of water or incompressible material into the joint, which can be problematic if there is limited edge drainage capability. Moreover, rocking of the slab caused by insufficient load transfer efficiency (LTE) and

poor base/subgrade support apparently resulted in significant faulting. If there is no strengthening of wet subgrade materials in the areas adjacent to the full depth repair (FDR), failure would soon spread to the adjacent areas as illustrated in the photographs.

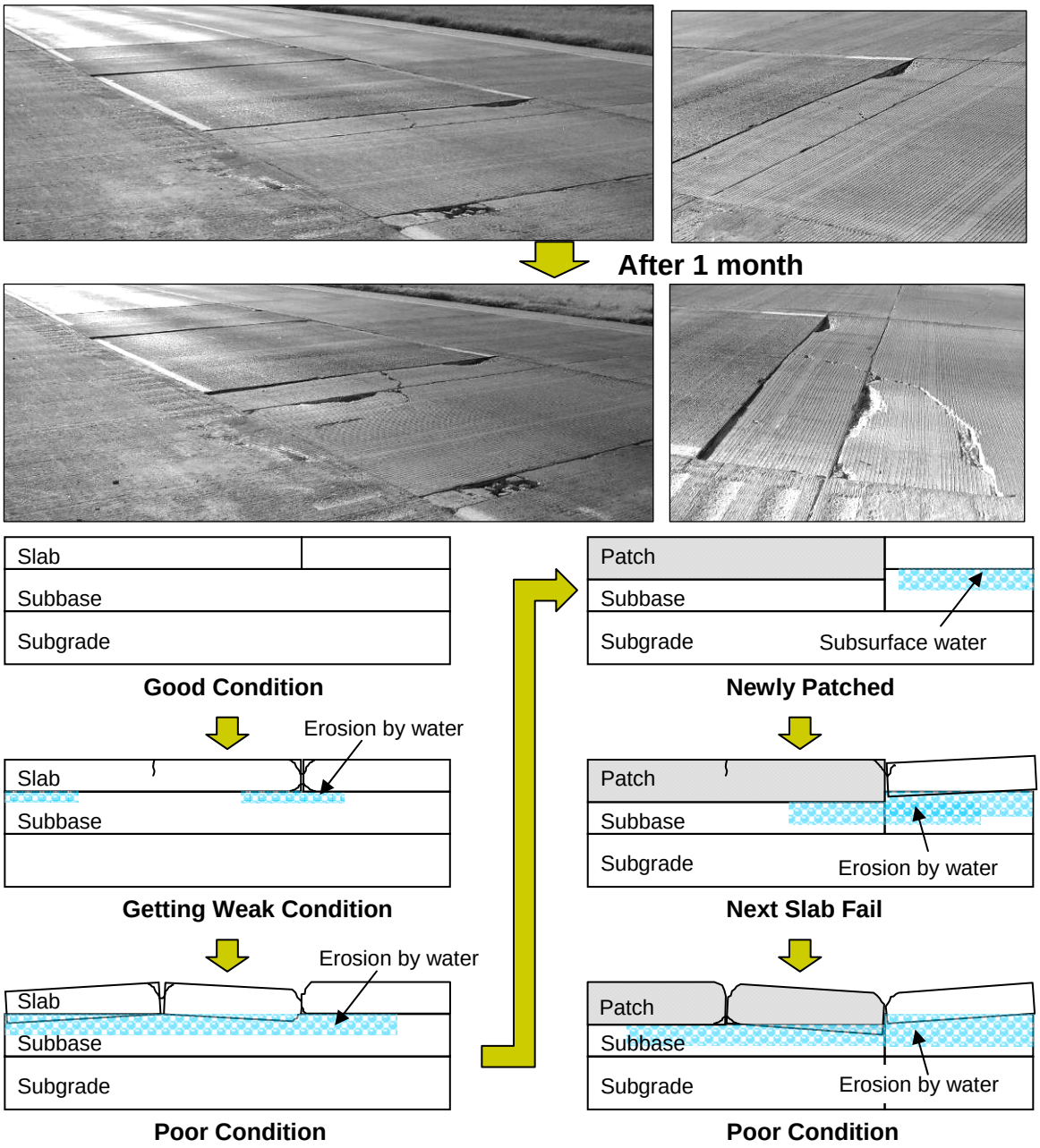

Figure 3 Subbase Erosion and Pavement Deterioration Process.

Ground Penetrating Radar Testing

Figure 4 shows GPR images where the black or dark areas represent voids and yellow or orange strips (white strip in the grayscale image) represent eroded or wet areas. Most sections showed voided and eroded areas in the subbase layer, while patched sections showed none (as expected) but slabs adjacent to the patched areas did indicate voided areas. The blue line at the bottom in Figure 4 indicates the dielectric value, which indicates the amount of accumulated moisture in the subbase. Our experience indicates when a dielectric constant (DC) value is higher than about 9, a wet condition or erosion on the subbase may exist; much of test sections showed a DC value higher than 9.

Falling Weight Deflectometer Testing

FWD testing is commonly used to check overall structural capacity such as slab stiffness, loss of support (voids), LTE of the joint, and effective thickness determinations. Although backcalculation analysis involves theoretical related assumptions, FWD test procedures are well established and relatively simple to apply for evaluation of pavement condition. Loaded and unloaded deflections across a joint or crack are used to determine the LTE using Equation 1:

$$LTE = \frac{d_U}{d_L} \times 100 \quad \textbf{(1)}$$

where: LTE = load transfer effectiveness (%)

d_U = deflection on the unloaded side of the joint or crack (mils)

d_L = deflection at the loaded side of the joint or crack (mils)

In conjunction with the LTE, the calculated effective thickness, h_e indicates areas of deterioration. The locations show low effective thicknesses are interpreted as areas of low stiffness. The deflection basin area (BA), based on seven sensors, is used to determine the effective radius of relative stiffness as a function of the effective thickness using Equation 2 (*1*).

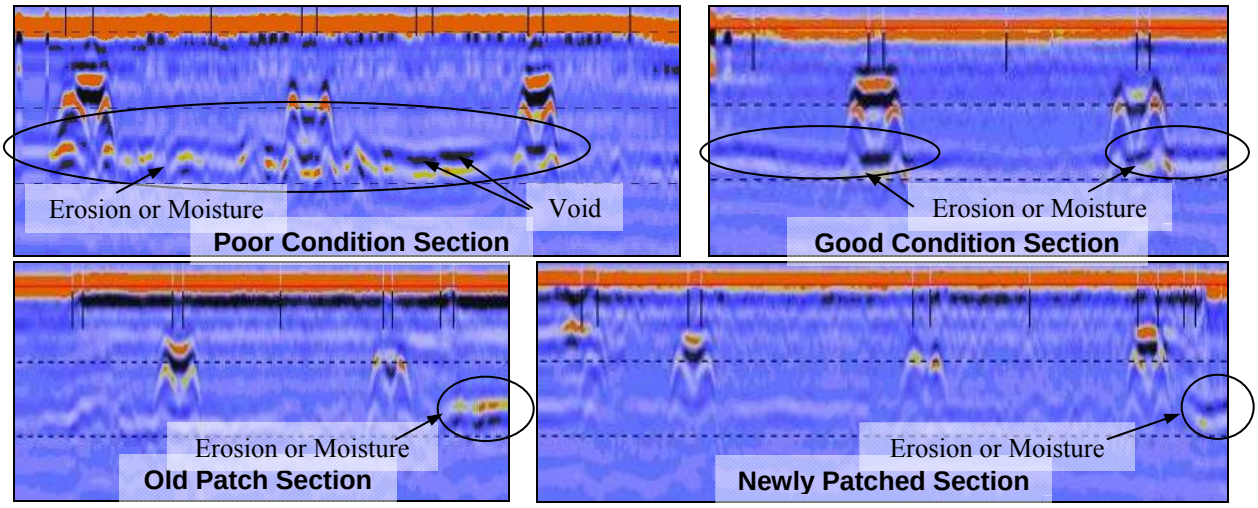

a) GPR along FWD Lane Center Drop Points (Ground-Coupled System)

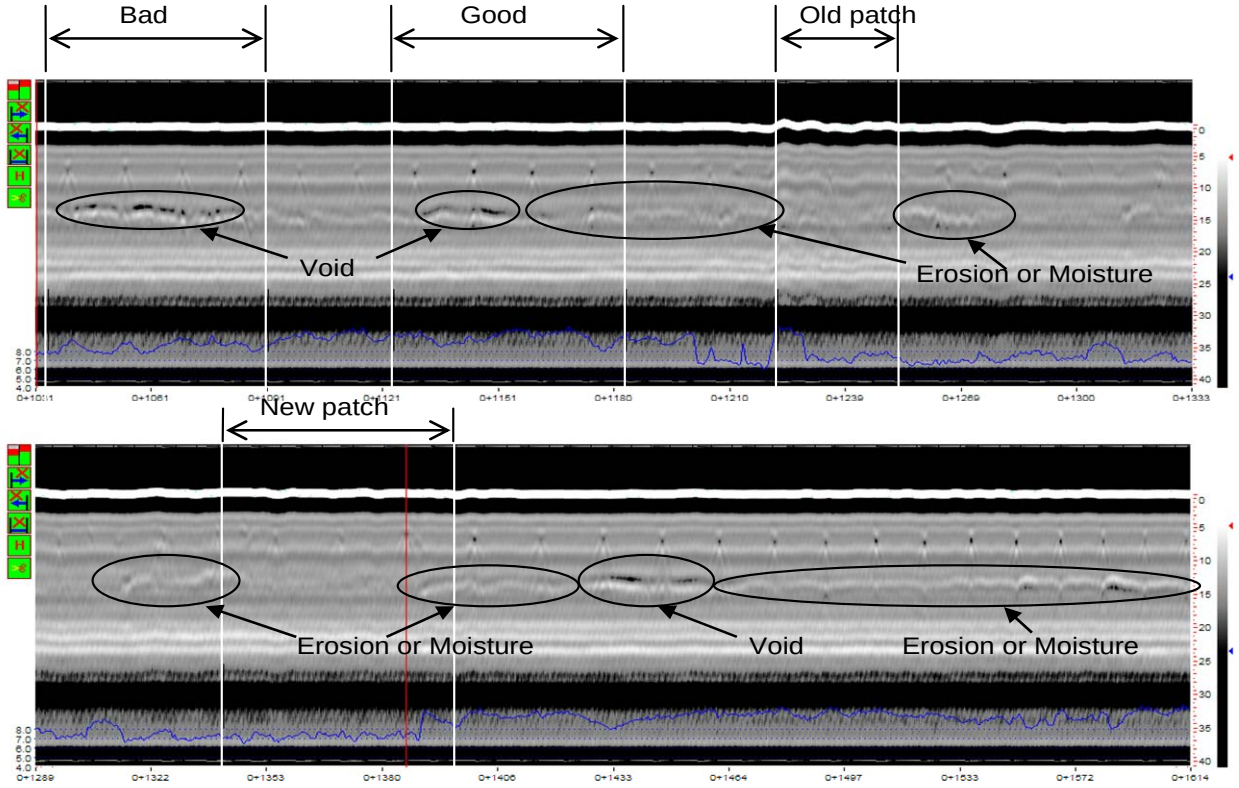

b) GPR along Edge Side Wheel Path (Air-Coupled Vehicle System)

Figure 4. GPR Images of Test Sections on US 75.

$$h_e = \left[\ell_m^4 \cdot \frac{12\left(1-\nu^2\right)k_{dyn}}{E_c} \right]^{\frac{1}{3}} \quad \textbf{(2)}$$

where:

h_e = effective slab thickness (in)

ℓ_m = radius of relative stiffness (in) = $0.0284 \cdot BA^2 - 0.2891 \cdot BA + 0.992$

ν = Poisson's ratio of the concrete

k_{dyn} = dynamic modulus of subgrade reaction (psi/in) = $\frac{d_0^* \cdot P}{d_0 \cdot \ell^2} \cdot 1000$

Ec = elastic modulus of the PCC layer (psi)

d_0^* = dimensionless deflection = $\frac{1}{8}\left[1 + \frac{1}{2\pi}\left(\ln\left(\frac{a}{2\ell}\right) - 0.673\right)\left(\frac{a}{\ell}\right)^2\right]$

P = wheel load (lb)

d_0 = deflection at the loading position (mils)

a = radius of loading plate (in)

BA = basin area calculated from 7 sensors (in)

$= 6\frac{d_0 + 2(d_1 + d_2 + d_3 + d_4 + d_5) + d_6}{d_0}$

d_1, d_2, d_3, d_4, d_5, d_6 = Deflection at 1, 2, 3, 4, 5 and 6 ft from the loading position (mils)

Figure 5 shows joint LTE and effective thickness along the center and the edge of slab. Interestingly, the patched sections had low LTE and effective thickness as if eroded conditions were present. The reason for low LTE in these sections is perhaps due to the lack of aggregate interlock along the joints. LTE and erosion are typically highly related to each other; joints with low LTE are often associated with high rates of erosion due to independent deflection behavior between two slabs; an eroded base also contributes to higher wear out rates of the aggregate interlock. Patches in pavements tend to create areas of low stiffness and consequently potential problem locations for future repair.

Figure 5. LTEs and Effective Thickness of Test Sections on US 75.

Dynamic Cone Penetrometer Testing

DCP testing indicates the in situ strength of the base and subgrade materials. It consists of upper and lower shafts. The upper shaft has a 17.6 lb drop hammer with a 22.6 in drop height and is attached to the lower shaft through the anvil. The lower shaft contains an anvil and a cone attached at the end of the shaft. The cone is replaceable and has a 60 degree cone angle. In order to run the DCP test, three operators were required. One person held the upper shaft, another person dropped the hammer, and the third recorded measurements. DCP testing seemed to be most useful on selected areas where visual and GPR surveys indicated evidence of pumping or subsurface water. Equation 3 shows the relationship between the penetration ratio (PR) and elastic modulus of soils (*2*).

$$E = 2550 \times CBR^{0.64} \quad \textbf{(3)}$$
$$CBR = 292 / PR^{1.12}$$

where: E = elastic modulus (psi)
CBR = California bearing ratio
PR = penetration ratio (mm/blow)

The base type for all sections investigated was an unbounded aggregate base (previously noted) where the estimated elastic moduli appeared to be quite low, as shown in Figure 6. Surprisingly, the base in the good performing areas was nearly the same modulus as that of the subgrade; perhaps the base material has been contaminated since

the elastic modulus for an unbounded aggregate base typically ranges from 15 to 45 ksi *(3)*. Patched areas showed a base modulus to be about twice the base modulus of the unrepaired sections. This causes discontinuous base support between the patch and adjacent sections which may contribute to slab cracking. There was no significant difference in the subgrade layer modulus.

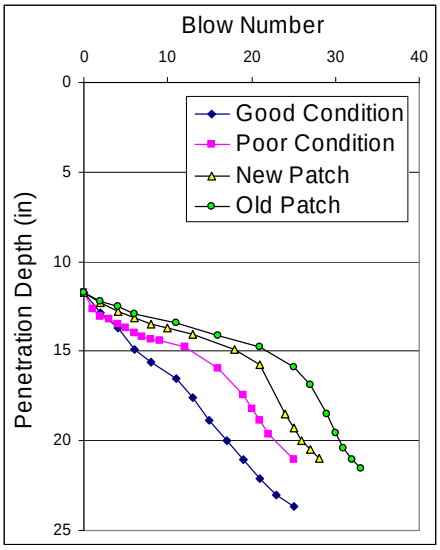

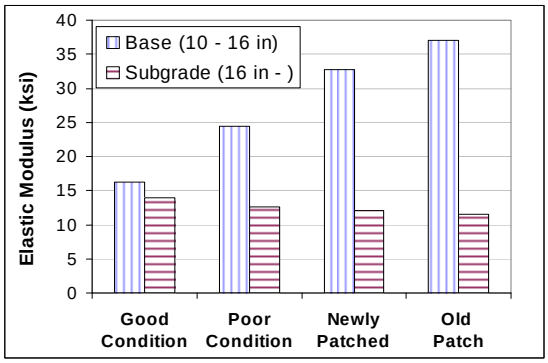

Depth	Good Condition	Poor Condition	Newly Patched	Old Patch
Base (10 - 16 in)	16.3 ksi	24.4 ksi	32.8 ksi	37.1 ksi
Subgrade (16 in -)	13.9 ksi	12.6 ksi	12.1 ksi	11.6 ksi

a) Penetration Ratio b) Elastic Modulus

Figure 6. DCP Testing Results of Test Sections on US 75.

Core Samples

Core samples provide a means to measure the compressive strength of the concrete and to indirectly estimate the modulus of the concrete layer relative to assessing the performance of the base layer. The core hole also provides a means of visually checking for voids and base erosion. The illustration shown in Figure 7 is of a cored location in a poorly performing section that exposes a voided area at the surface of the base layer due to erosion. Although not entirely evident, Figure 7 also shows the bottom surface of individual cores where the bond between the concrete and the base was observed after removal of the core. The core sample from the poor condition section showed evidence of separation (possibly due to erosion and pumping action), while the

sample from the good condition section showed partial bonding between the concrete slab and the base. Cores from patched areas did not show evidence of separation.

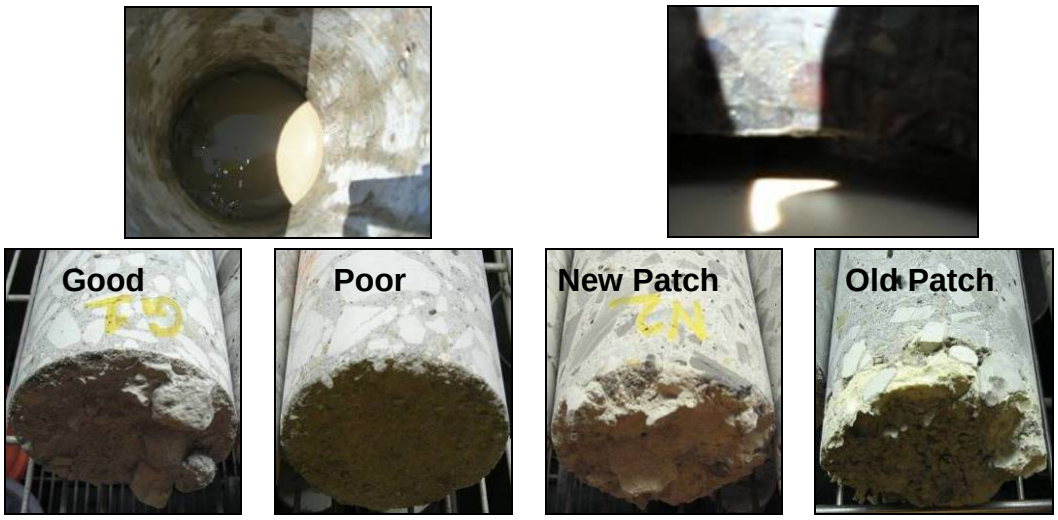

Figure 7. Erosion under the Concrete Slab and Cored Sample of Sections on US 75.

US 81/287—WISE COUNTY

Sections on CRC pavement on northbound US 81/287 near Decatur, TX were sampled to monitor base or subgrade erosion performance. Traffic was noted to be 23,000 average daily traffic (ADT) which is estimated to be 1.7 million equivalent single axle load (ESAL) per year (with 23 percent trucks), with an estimated 20 million historical ESAL. Figure 8 shows a distressed typical area of each section and Table 3 shows visual survey results of Section 2.

Sections 1 and 2, constructed in 1971, consisted of 8 in CRC pavement over a 4 in AC base and a 6 in lime-treated subgrade (LTS). The pavement had an AC shoulder and showed some evidence of pumping and patching. The crack pattern was fine but the widths of the cracks appeared to be wide in many areas due to the use of a Skidabrader to address surface friction issues. Some of patched sections showed faulting distress at the joints.

Sample Section 3, located 1 mi to the north was opened to traffic in 1985. This section consists of a 12 in CRC pavement over 4 in AC base (double layer of 2 in

thick AC) and a 6 in LTS. Performance has been reasonably good. The pavement also has a 3 ft extended concrete lane as part of the shoulder; the remaining shoulder is AC and the longitudinal joint between the AC and PCC is well sealed, effectively blocking intrusion of water into the pavement section.

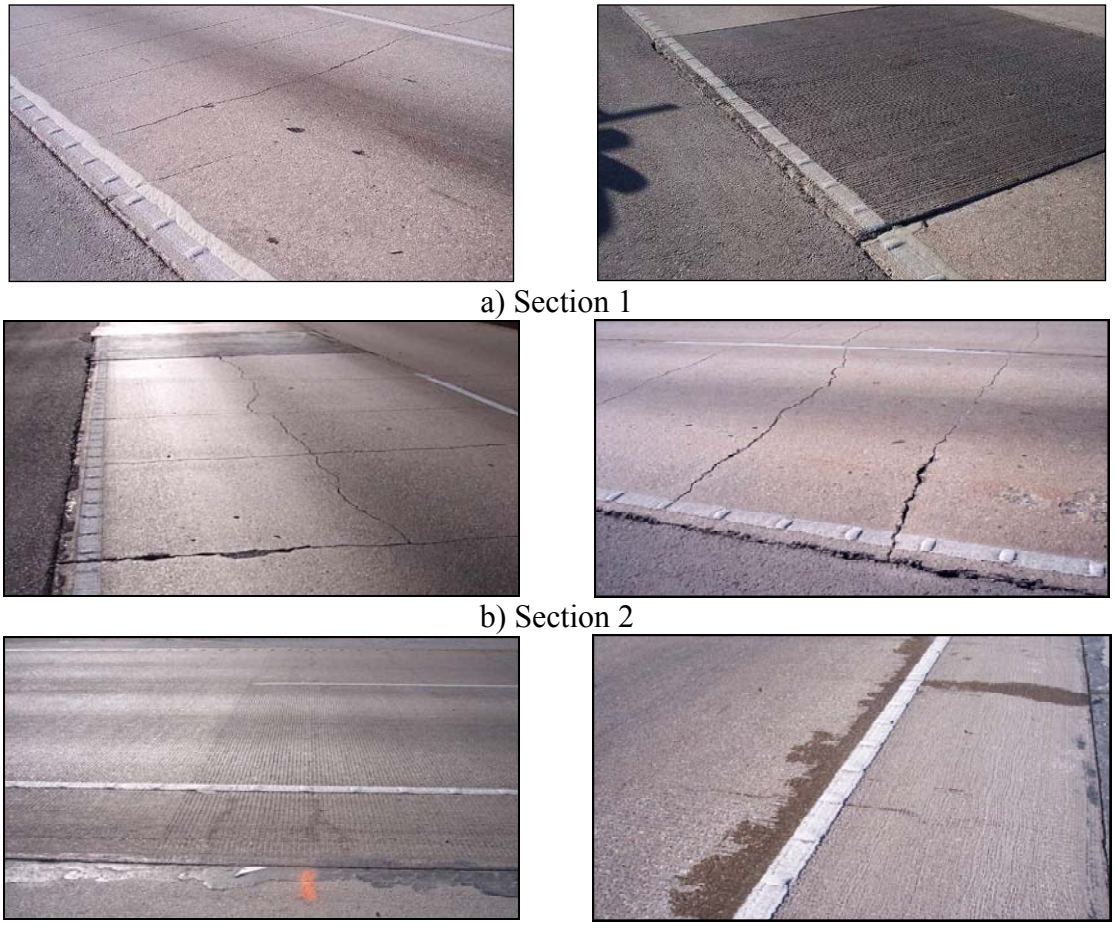

a) Section 1

b) Section 2

c) Section 3

Figure 8. Test Sections on US 81/287.

Ground Penetrating Radar Testing

Figure 9 shows GPR images where blue areas represent voids and red areas represent eroded or wet condition areas. Generally, the images indicate that the interface between the AC base and the lime-treated subgrade is wet throughout much of the sample section.

Table 3. CRC Pavement Condition Survey of US 81/287 (Sample Section 2).

No.	Checklist	Notes
1	Pavement age (yr)	37 yr 8 in CRC pavement
2	Aggregate type (hard or soft)	Soft — limestone
3	Year of recent pavement distress survey (yr)	N/A
4	Year of recent pavement deflection survey (yr)	N/A
5	Joint sealant age (yr)	N/A
6	Sealant damage of transverse joint (%)	N/A
7	Sealant damage of longitudinal joint (%)	70%, No seal on shoulder
8	Sealant damage of sealed crack (%)	N/A
9	Trapped surface water in depressed area	No
10	Standing water or slab staining	No
11	Pumping with or without staining	Positive
12	Bump (stable or unstable; depth, in)	No
13	Settlement (stable or unstable; depth, in)	No
14	Joint spall (width, depth, % of joint spall > 2 in)	N/A
15	Crack spall (width, depth, % of crack spall > 2 in)	2 in, 3/4 in, 20% 1/4 in, 1/2 in, 80%
16	Deep spall (depth, in)	No
17	Patching (number/mi)	7
18	Faulting (depth, in)	Patched area 0.5 in
19	Longitudinal crack (width, number/slab)	0.05 in, 1/over 4 cracks, 20 ft length
20	Shoulder separation (width, in)	1/2 in, No joint seal
21	Punchout (spall width, fault depth, % of slab)	No

GPR images of Section 1 showed significant amounts of wet or eroded areas in the lime-treated subgrade layer; however, little erosion on the AC base layer was detected. GPR images of Section 2 showed some erosion between the concrete slab and the AC layer, which was verified by coring. Wide crack widths, no longitudinal joint sealing as well as a wide shoulder joint possibly contributed to the occurrence of erosion. Even though GPR images of Section 3 showed a low level of moisture at the interface between two AC base layers and a moderate level of moisture on the subgrade layer, no significant erosion was identified.

DC trends in the subbase layers of Sections 1 and 2 show relatively high DC values (around 8 to 10), while Section 3 DC values indicate lower moisture levels (around 7).

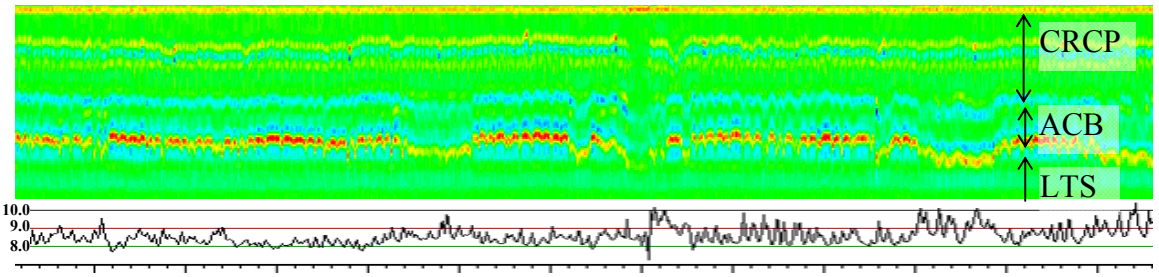

Section 1

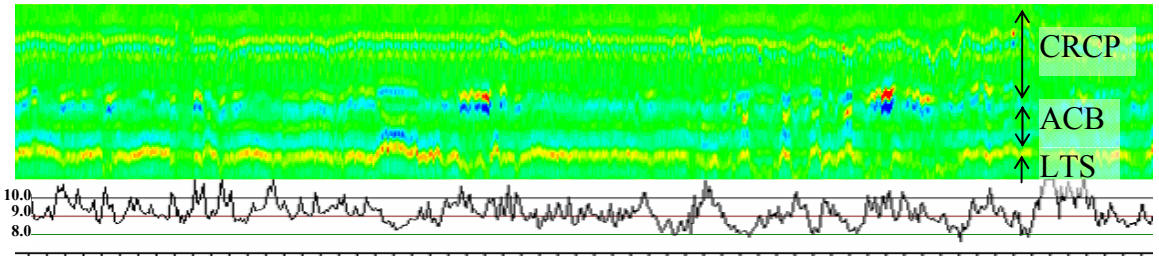

Section 2

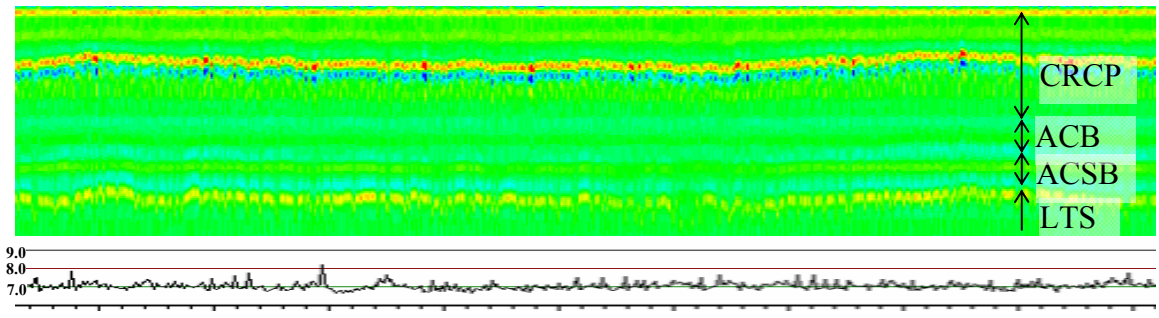

Section 3

Figure 9. GPR Images of Test Sections on US 81/287.

Falling Weight Deflectometer Testing

FWD testing was conducted along the wheel path (1.5 ft inside from pavement edge) in each section where the associated deflections are shown in Figure 10. As expected, Sections 1 and 2 showed higher deflections (about 6 times higher) than those measured in Section 3 since the concrete slab thickness is less. However, Section 1 showed a greater mean deflection than those noted for Section 2 even though these sections have the same layer thickness; the difference may be due to wetter subgrade conditions based on the GPR results.

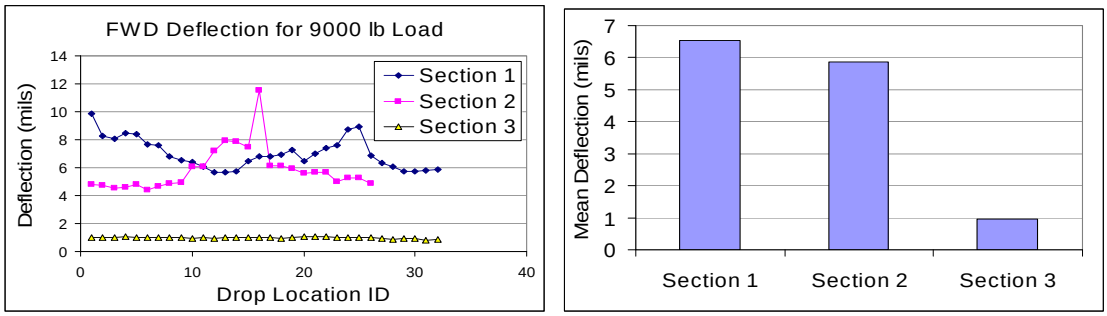

Figure 10. Deflections of Test Sections on US 81/287.

Figure 11 shows the mean section LTE and effective thickness. Section 3 shows lower LTE than the other sections even though this section has greater effective thickness. The pavement stiffness of this section is good, perhaps since the subgrade conditions are drier based on the GPR results; however, erosion between the AC base layer and the lime-treated subgrade was detected from the core sample. Sections 1 and 2 show good overall LTE and effective thickness, but some cracks have a relatively low LTE and may hold a higher possibility of erosion in the future at those locations.

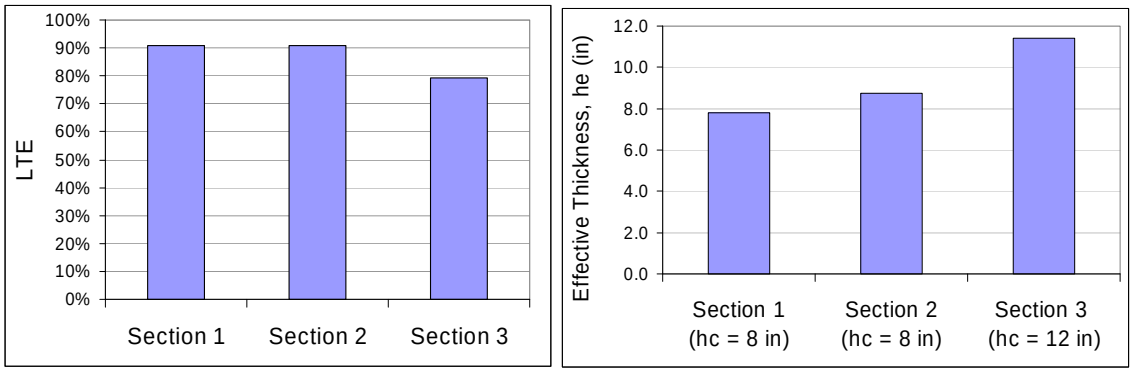

Figure 11. LTEs and Effective Thicknesses of Test Sections on US 81/287.

Figure 12 suggests evidence of subgrade erosion in portions of Sections 1 and 2. Combinations of low effective thickness and high deflections usually suggest that the base or subgrade layer could be eroded. Moreover, a high deflection condition means greater chance of mechanical and hydraulic shearing action taking place at the interface between the slab and the base under the effect of applied loading. If the LTE is high, erosive action would be reduced, but when LTE is diminished at a crack or joint, the independent vertical movements of adjacent slabs could accelerate the erosion process. The location of low effective thickness and high deflection noted in Section 2 was matched to the wet area noted by the GPR data as well as being verified through coring.

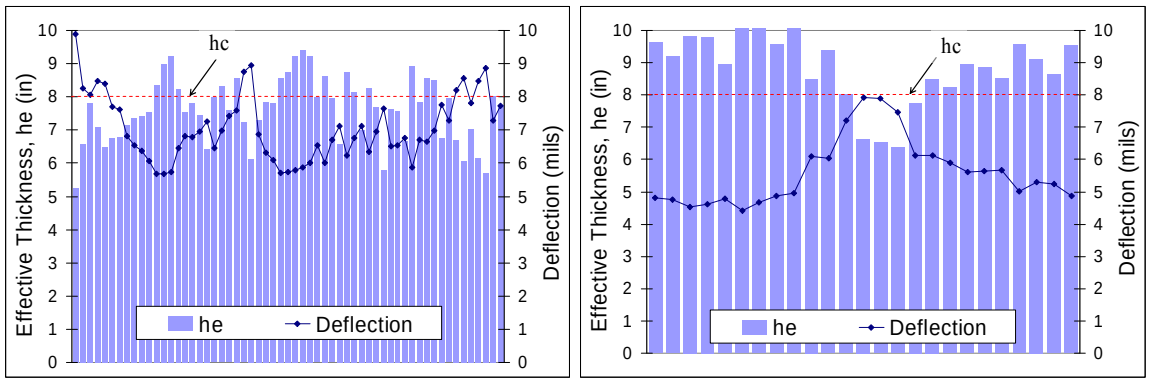

Figure 12. Effective Thicknesses and Deflections of Test Sections on US 81/287.

Dynamic Cone Penetrometer Testing

All sections were constructed over a 6 in lime-treated subgrade. Figure 13 shows DCP results from the three sample sections. Section 1 has the lowest elastic modulus, perhaps due to the wet subgrade conditions as noted by the GPR images. Section 3 showed the highest modulus although it is in the low end of the range of typical values. The natural subgrade material (sandy soil) is perhaps a low modulus material with a low resistance to erosion.

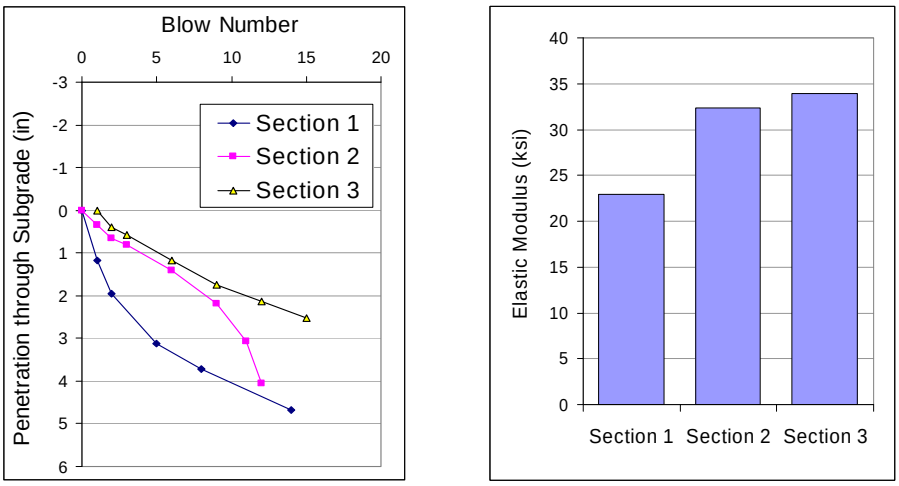

a) Penetration Ratio of Lime-Treated Subgrade

b) Elastic Modulus of Lime-Treated Subgrade

Figure 13. DCP Testing Results of Test Sections on US 81/287.

Core Samples

Figure 14 shows core samples taken from Section 1 and a view of the interface condition between the AC base and the subgrade. Contact between the concrete slab and the AC base was good with little wear within the sample. However, some erosion at the interface between AC and subgrade was detected as shown.

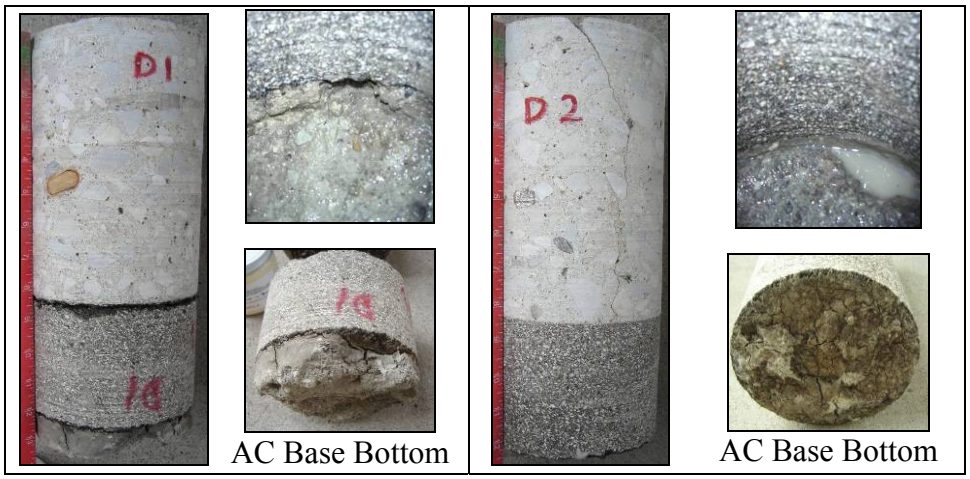

Figure 14. Cored Samples and Subgrade Condition of Section 1 on US 81/287.

Sampling in Section 2 indicated a higher level of erosion between the concrete slab and the AC base as shown in Figure 15. The core was located on the transverse crack, but the longitudinal joint between lane and shoulder lacked a joint sealant increasing the propensity for water to intrude the pavement structure and contribute to erosion at the surface of the AC base. The bond between AC base and subgrade was clearly missing as there was light erosion on the interface.

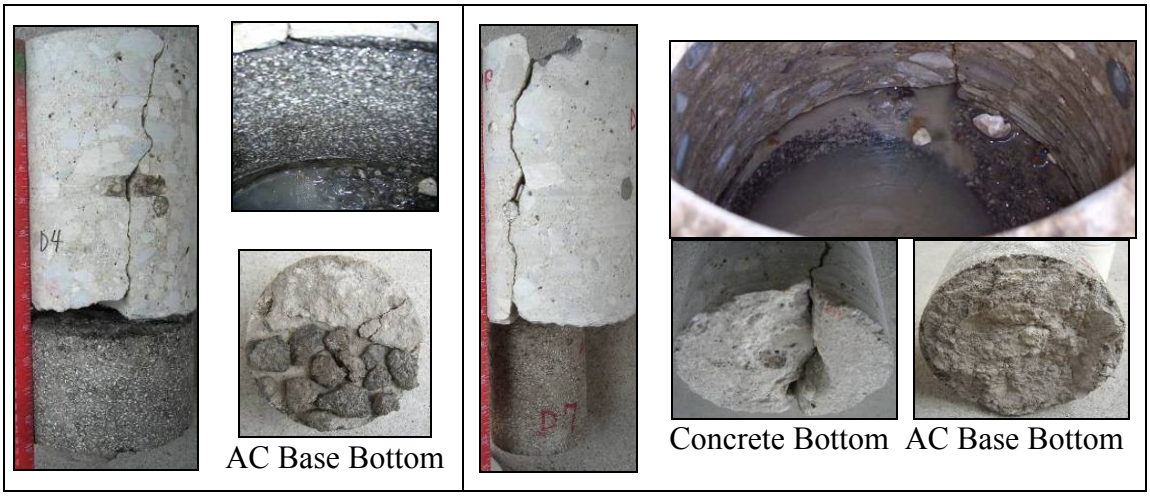

Figure 15. Cored Samples and Subgrade Condition of Section 2 on US 81/287.

The core from Section 3 shown in Figure 16 manifest erosion on the AC subbase layer; the bond condition between PCC and AC base layer was good, but the debonding and the erosion between two AC layers diminishes the structural integrity of the pavement. The subgrade layer did not show significant erosion even though it was debonded with the AC subbase. Nonetheless, this section presently manifests a relatively high effective thickness but with the joint seal being in good condition has helped maintain a sound subgrade condition with voiding beneath the base.

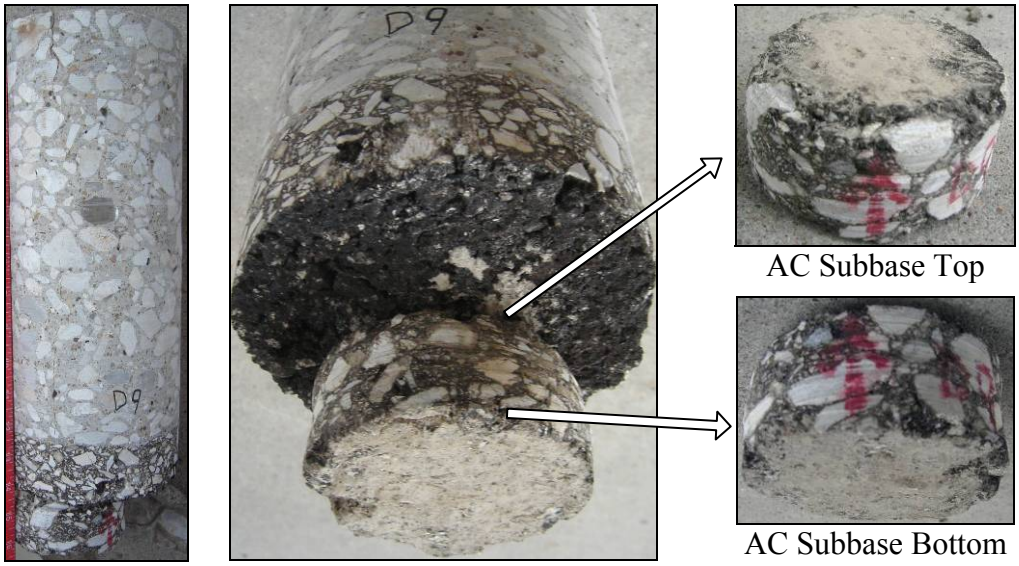

Figure 16. Cored Samples and AC Base Condition of Section 3 on US 81/287.

FM 364—BEAUMONT AREA

A sample section on FM 364 in Beaumont consisted of a jointed 10 in thick pavement with a 15 ft joint spacing over 6 in cement stabilized oyster shell base. It was opened to traffic in 1985 and current traffic is 21,000 ADT with 2.5 percent trucks. Figure 17 shows the surface condition of the sample section. Some slabs had transverse cracks near the joints (about 1 ft apart) possibly due to late sawcutting. The joint seal condition was generally good, but not all the cracks were sealed properly promoting water intrusion and erosion of the base.

Figure 17. Surface Conditions of Sampled Section on FM 364.

Ground Penetrating Radar Testing

Core sampling was selected based on the presence of the red strip in the GPR image (Figure 18) as an indication of erosion-related damage. However, moisture was scarcely present in the base, where there was little evidence of erosion damage. DC values were around 7 to 9 and fluctuated as shown at the bottom of the scanned image

suggesting a high chance of water being present at the interface of the slab and base layer.

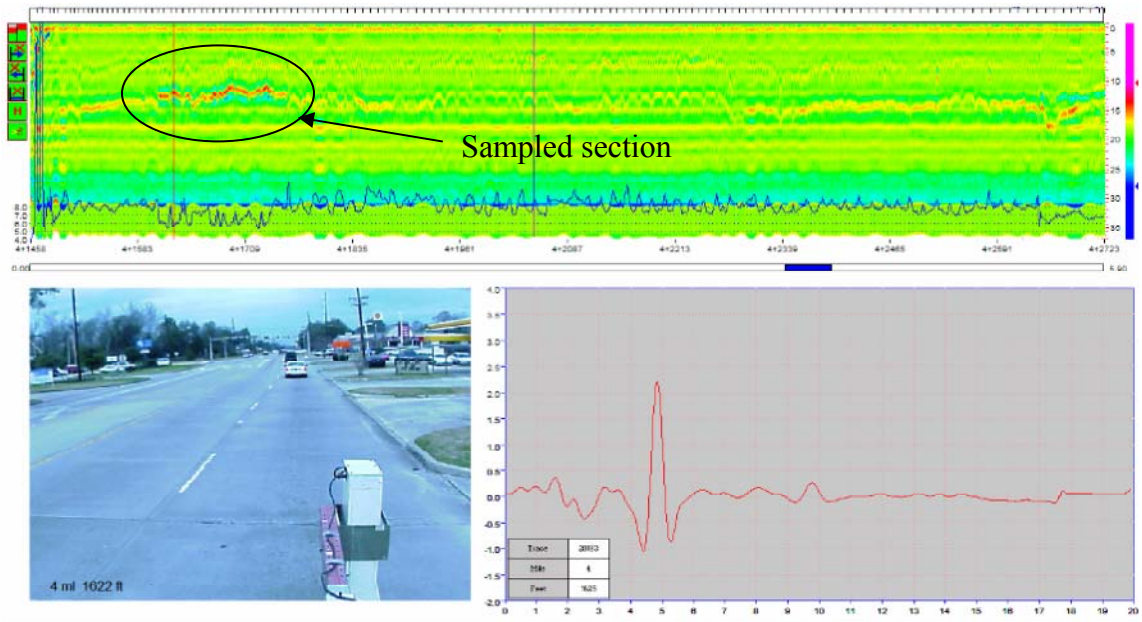

Figure 18. GPR Image of Test Section on FM 364.

Falling Weight Deflectometer Testing

FWD testing was employed in the outside wheel path of the outside lane since there is no shoulder; Figure 18 shows the LTEs, effective thickness, and deflections. Most joints show good LTEs and deflections in the range of interior loading conditions. Effective thickness and deflection data is shown in Figure 19. As discussed before, low effective thickness with high deflection are indicators of erosion damage at that location, which was verified through the coring.

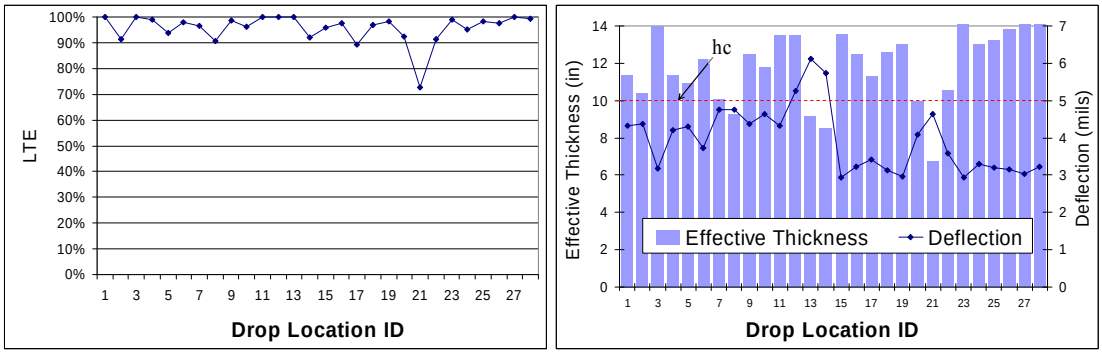

Figure 19. LTE, Effective Thicknesses, and Deflection of Test Section on FM 364.

Dynamic Cone Penetrometer Testing

Figure 20 shows DCP results from two core holes made on site. Calculated modulus was around 12 ksi which is in the normal range of subgrade material moduli (3 to 40 ksi).

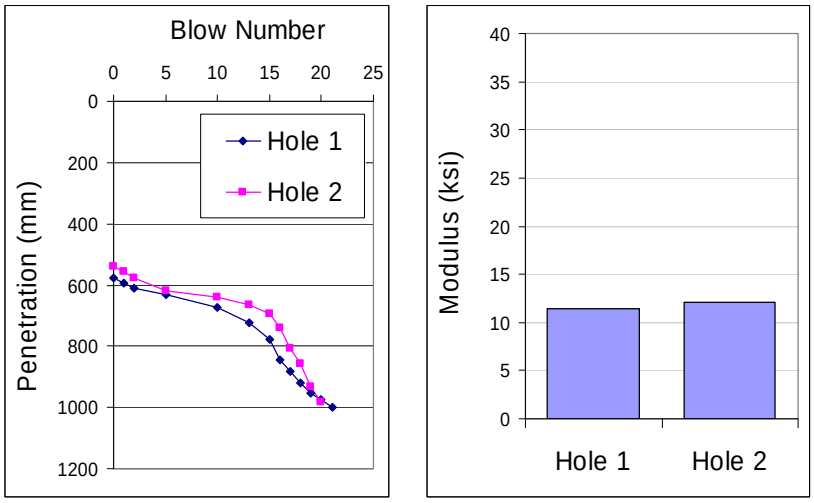

Figure 20. DCP Testing Results of Test Section on FM 364.

Core Samples

Figure 21 shows views of the interface condition of all the layers in the pavement. Erosion was detected at the interface between the PCC and the cement stabilized oyster shell base near the joint but no erosion was noted away from the joint as indicated by the good contact between the concrete slab and the base. Water intrusion near the joints probably contributed to erosive action but the damage at the interface between base and

subgrade was limited to the vicinity of the joint. The bottom of each layer as shown indicates a debonded condition.

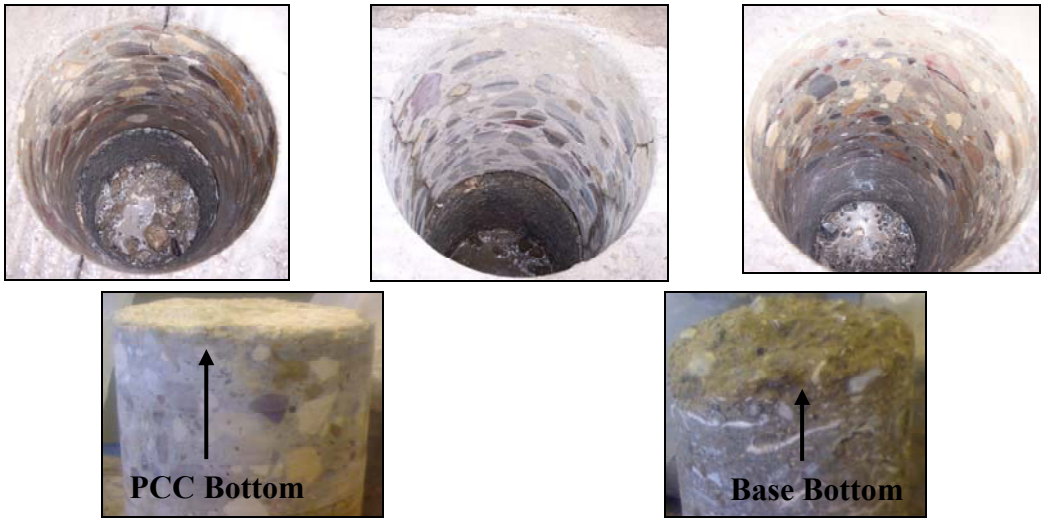

Figure 21. Interface and Subgrade Condition of Section on FM 364.

IH 10—BEAUMONT AREA

The support conditions of a frontage road along IH 10 located in Beaumont, TX, which consisted of a 6 in CRC pavement over silty and sandy subgrade (no base layer) that was constructed in 1963 was investigated. The pavement carries approximately 100 ADT with 3.2 percent truck traffic. Distressed areas indicate signs of overloading are shown in Figure 22 and consist of severe map cracking with spalling and pumping. Joint or crack sealing was practically nonexistent and the pavement was severely deteriorated in the vicinity of the expansion joints. Some patched areas had settled and broken at the corner or in the wheel path; areas adjoining to the patches typically had low LTE and poor support. Most of the damage appeared to be due to a weak subgrade.

Ground Penetrating Radar Testing

Most of the survey sample area showed a high degree of moisture and voiding under the slab based on the GPR results in Figure 23. DC values were around 7 to 9 and fluctuated (with high DC values near crack locations) as shown at the bottom of the

scanned image. Some peaks occurring at the beginning and end of the FDR patches may indicate the presence of moisture (there was no joint seal between patches and surrounding pavement) possibly leading to more settlement and discontinuous support conditions.

Figure 22. Surface Conditions of Sampled Section on IH 10.

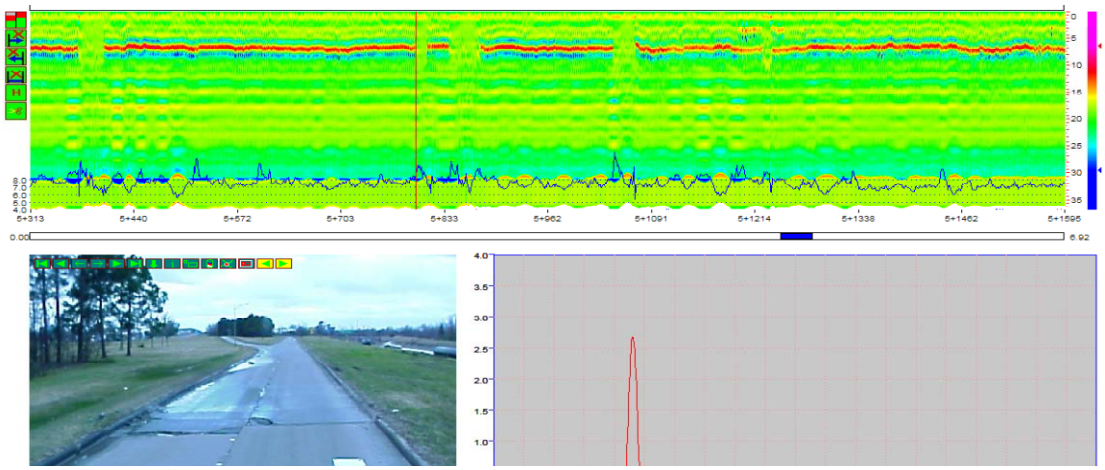

Figure 23. GPR Image of Test Section on IH 10.

Falling Weight Deflectometer Testing

Figure 24 shows the deflections and LTEs from FWD testing along the center of the outside wheel path of the sampled section lane. FWD testing on the approach side of the patched area showed more uniform and lower deflection conditions compared with the leave side of the patch because the approach side consisted of tighter cracks which did a better job of shedding water off the pavement surface. LTE was generally good (even though deflections were high) except at the FDR joints. Effective thickness trends were similar as the deflection trends. Low effective thickness in combination with high deflection was found at the FDR patch joints indicating weakened subgrade conditions at those locations.

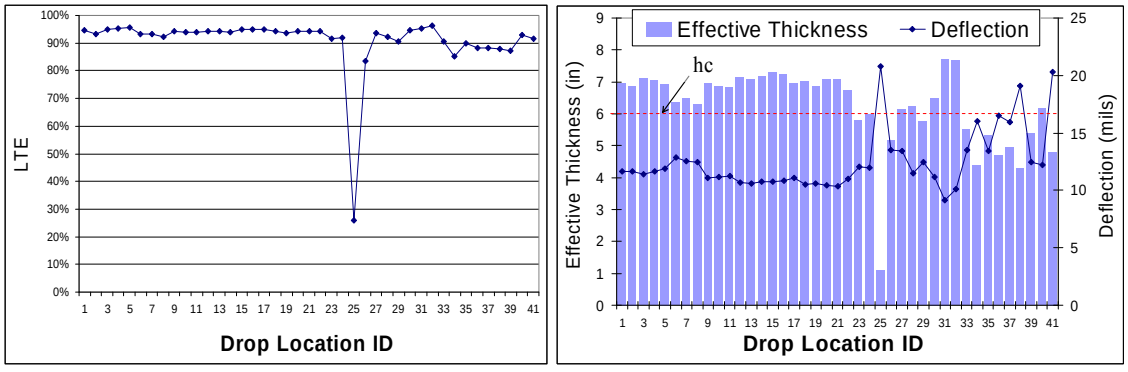

Figure 24. LTE, Effective Thicknesses, and Deflection of Test Section on IH 10.

Dynamic Cone Penetrometer Testing

Figure 25 shows DCP results from four core hole locations. All four tested locations showed very high penetration ratios through the top 12 in Calculated moduli were around 2.5 to 3 ksi. The subgrade is very weak; however, smaller penetration ratios were detected below 14 in from the top of the subgrade layer (calculated moduli were approximately 12 to 13 ksi) indicated this part of subgrade was highly saturated.

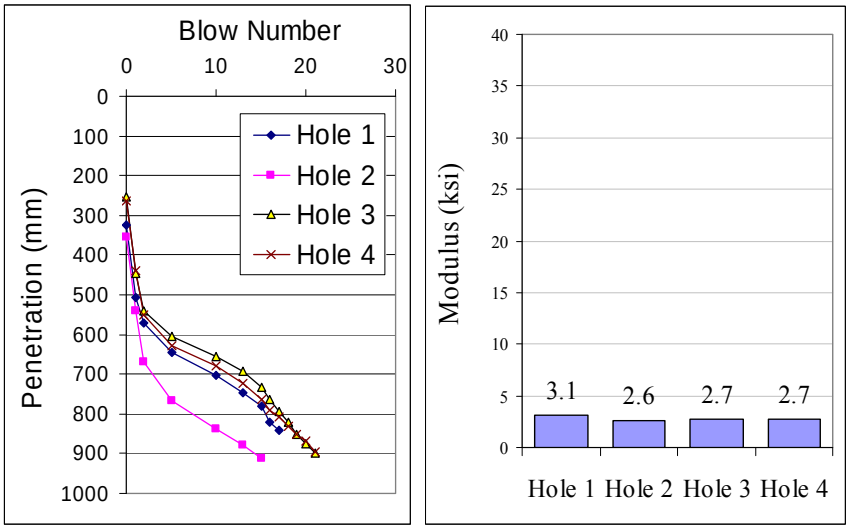

Figure 25. DCP Testing Results of Test Section on IH 10.

Core Samples

All four cores showed eroded conditions and, of course, no bonding between the concrete and the subgrade (Figure 26). Since there is no base layer, subgrade material was directly subjected to subsurface water through cracks and spalling in the concrete surface exposing it to pumping action and vehicle loading. However, pumping was not excessive since the traffic loading was only approximately three trucks per day. The coring in Figure 26 shows horizontal cracking along the reinforcing bar.

Figure 26. Interface and PCC Layer Condition of Section on IH 10.

IH 635—DALLAS AREA

A CRC pavement section on IH 635 from IH 35E to US 75 was sampled to evaluate the base condition. Sampled sections consist of an 8 in CRC pavement with a concrete shoulder over a 4 in CSB that was opened to traffic in 1967 that currently carries an ADT of 200,000 with 12 percent trucks. Surface conditions shown in Figure 27 were generally good except some spalled cracks and patchs. The key distress types are the full-depth patches and the widened longitudinal joints although the overall condition of the pavement appears to be very good. The patches in the pavement are most likely repairs of punchout distress that are possibly a result of erosion and loss of support immediately below the slab since widened longitudinal joints are evident at a few locations. The patch density is not high, but in places, it is as high as 5 per mile.

Ground Penetrating Radar Testing

GPR image in Figure 28 showed some moisture areas under the concrete slab but no significant sign of erosion was identified. DC values of overall sections are around 7 to 8 representing a low level of moisture on the base layer.

Figure 27. Surface Condition of Sampled Section on IH 635.

Figure 28. GPR Image of Sampled Section on IH 635.

Falling Weight Deflectometer Testing

The results of FWD testing along the wheel path of the outside lane shown in Figure 29 indicates good LTEs but there are a few areas where low values of effective thickness exist indicating the integrity of this pavement is beginning to diminish although the performance over the life of this pavement has been very good. Where effective thickness is less than the existing concrete slab thickness indicates a lack of support possibly due to erosion of the base.

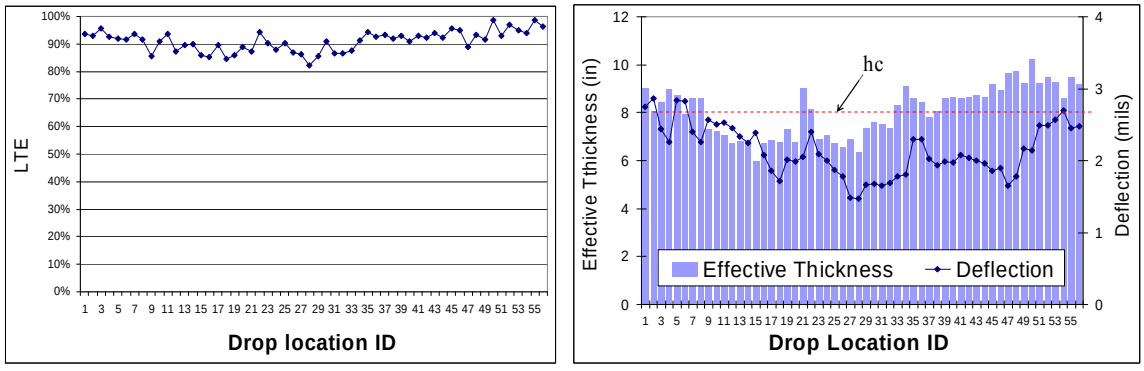

Figure 29. LTE, Effective Thicknesses, and Deflection of Test Section on IH 635.

Dynamic Cone Penetrometer Testing

DCP testing was performed at core locations to assess the insitu strength characteristics of undisturbed soil and/or compacted materials below the subbase. The results of six representative holes in Figure 30 show good subgrade conditions except for one area showing a calculated modulus of 12.4 ksi.

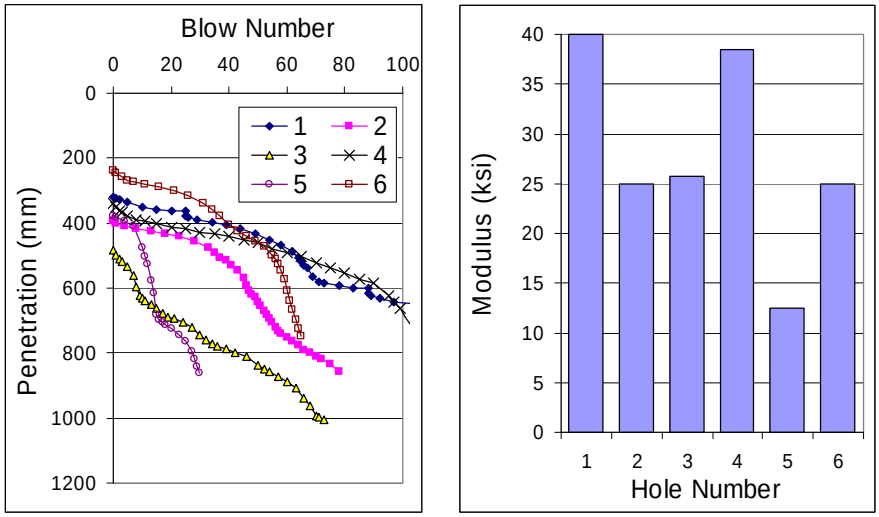

Figure 30. DCP Testing Results of Test Section on IH 635.

Core Samples

Erosion was found only at areas where the condition of the longitudinal construction joint was not well maintained and moisture had penetrated the pavement (Figure 31). The stabilized base consisted of cemented sand with gravel and ranged in thickness from 3 to 5 in, while the subgrade mainly consisted of clay material. The pavement support is not presently as issue but could soon become serious if maintenance activities are terminated or diminished for an extended period of time. Life extension could be facilitated by addressing the areas in the pavement structure that do not drain well and allow water to penetrate below the surface of the pavement.

Figure 31. Cores of Sampled Section on IH 635.

CHAPTER 3
EROSION MECHANISM

The shear stress or water under pressure from a moving load along the interface between concrete slab and base layer plays a major role in the erosion process. As the stiffness of the joint or crack decreases, the slab shear stress increases under the applied loading generating fines along the slab-subbase interface, which are susceptible to dislocation under pressurized water movement via pumping through joints or cracks to the pavement surface. Pumping can grow a void under the slab eventually leading to a loss of joint stiffness; this sequence is also accelerated by mutual effects.

Figure 32 shows conceptually the action of pumping at the corner of a concrete slab (*4*). The water induced shear stresses on the subbase are developed based on the slab movement simulated by a stiff plate rotating about an axis. The initial edge gap, H, is attributed to curling and warping of the concrete pavement.

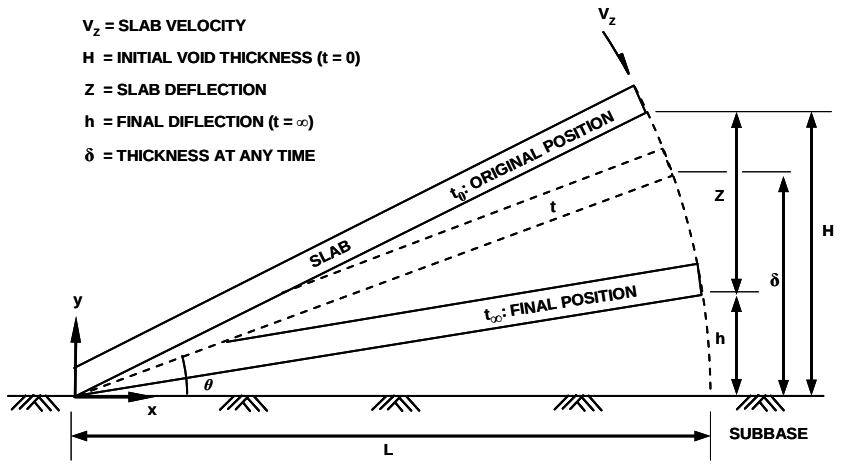

Figure 32. Slab Configuration of Erosion Modeling by Pumping (*4*).

Phu and Ray identified water velocity with respect to three void thickness zones in which water behaves differently according to theoretical, laboratory, and in-situ observations. Water behaves as a viscous fluid in the void less than 20 mils while it behaves as an ideal fluid in the void larger than 40 mils in thickness. Water velocity was

calculated by different equations for each condition and the interpolated water velocity was applied for transition zone voids between 20 and 40 mils. Maximum shear stresses in Figure 33 were obtained from ideal fluid conditions which drop with an increase of void thickness, but increases with vehicle speed (*5*). Since the slab is not deflected at a constant velocity, the resistance of water reduces slab speed and shear stress with void thicknesses less than 40 mils. On the other hand, fluid pressures drop significantly when the void thickness exceeds 40 mils, but that pressure increases with vehicle speed.

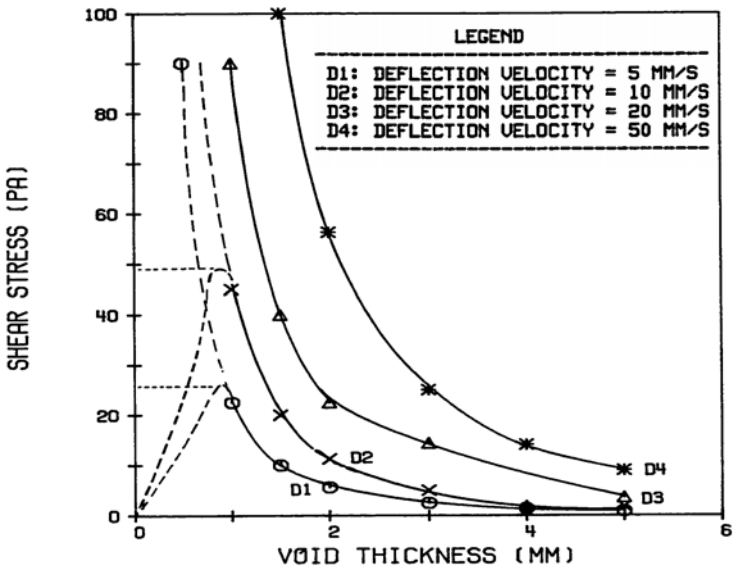

Figure 33. Effect of Void Size and Velocity of Slab Deflection on the Shear Stress (*5*).

Figure 34 shows the schematic view of the stress distribution of the approach slab under loading and generating fines by a deflection induced shear at the interface. The thermal movement of concrete on the opening and closing of the joint along with repeated loading across the joint diminishes the load transfer between adjoining slabs while enhancing the independent deflection movement of the slab. In the case of bound bases, the frictional interface is a key factor in the deterioration process. A stiff base causes high frictional stress along the interface especially at the corner of the slab. This frictional stress generates mechanical abrasion or fracturing when the shear stress

exceeds the shear strength of material. Unbound material bases may deform under slab deflection generating internal friction through aggregate-to-aggregate contact inducing fine material internally.

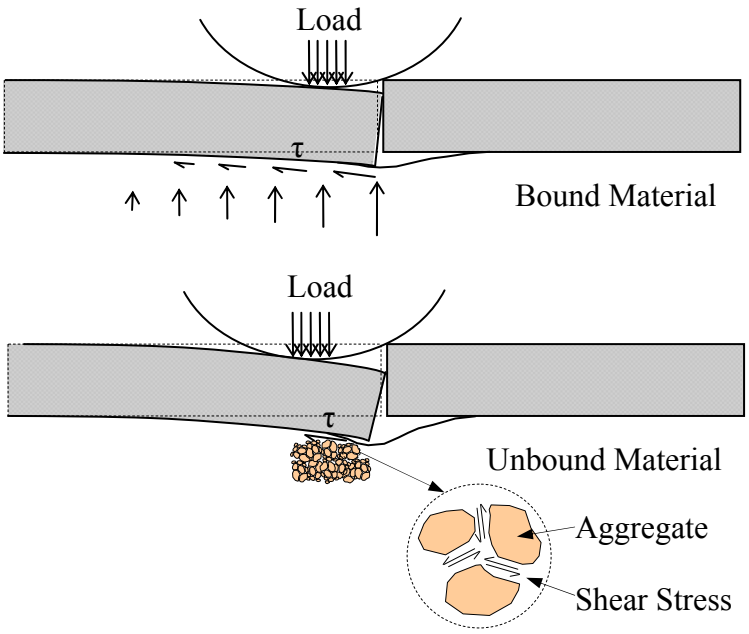

Figure 34. Shear Induced Erosion.

CHAPTER 4
EROSION IN DESIGN PROCEDURES

The erosion of material beneath the slab is an important performance-related factor that needs to be addressed in the selection of base materials as part of the design process for concrete pavements. In this regard, general design factors such as concrete slab stiffness, traffic, environmental factors, and strength and abrasion resistance (or shear strength) of the base and sugrade materials should be considered relative to erodibility. Moreover, drainage and layer frictional conditions should be considered in the design process in order to consider the full extent of erosion damage. As background, past and current methods (including models) relative to erosion are reviewed (*6*).

PCA DESIGN METHOD

The Portland Cement Association (PCA) procedure, subbase erosion is related to pavement deflection (at the slab corner) due to axle loading. Equations 4 and 5 were developed based on the results of the American Association of State Highway and Transportation Officials (AASHO) Road Test for allowable load repetitions and erosion damage:

$$\log N = 14.524 - 6.777(C_1 P - 9.0)^{0.103} \quad \textbf{(4)}$$

$$\text{Percent erosion damage} = 100 \sum_{i=1}^{m} \frac{C_2 n_i}{N_i} \quad \textbf{(5)}$$

where: N = allowable number of load repetitions based on a pressure of 3.0 psi

C_1 = adjustment factor (1 for untreated subbase, 0.9 for stabilized subbase)

P = rate of work or power = $268.7 \frac{p^2}{hk^{0.73}}$

p = pressure on the foundation under the slab corner in psi, $p = kw$

k = modulus of subgrade reaction in psi/in

w = corner deflection in in

h = thickness of slab in in

m = total number of load groups

C_2 = 0.06 for pavement without concrete shoulder, 0.94 for pavements with tied concrete shoulder

n_i = predicted number of repetitions for ith load group

N_i = allowable number of repetitions for ith load group

Separated sets of tables and charts are used for doweled and aggregate interlock joints with or without concrete shoulders. Since the erosion criterion was developed primarily from the results of the AASHO Road Test using a specific subbase that was highly erodible, the application of the model is limited as far as application to different subbase types. Nonetheless, this procedure represents a significant advancement in the mechanistic analysis of pavement support condition in design.

AASHTO DESIGN METHOD

Potential loss of support (LS) due to foundation erosion is utilized as input to effectively reduce the modulus of subgrade reaction in the thickness design procedure relative to four different contact conditions (i.e., with LS = 0, 1, 2, and 3). The best case is LS = 0, when the slab and foundation are assumed to be in full contact, while the worst case is LS = 3, when an area of slab is assumed not to be in contact with the subgrade (thus reduced values of k-value are in effect).

In Table 4, the possible ranges of LS factors for different types of subbase materials are provided to adjust the effective modulus of reaction. The subjectivity of the model reduces its sensitivity to material factors associated with erosion leading to inconsistency and limiting applicability. Load transfer coefficient and drainage coefficient are also indirectly related with erosion; a lower deflection caused by better load transfer would reduce shear stress at the interface between the slab and base/subgrade as well as a shorter time of water presence due to better drainage may decrease the potential for pumping. Therefore, major factors causing erosion can be considered in the design.

Table 4. Typical Ranges of LS Factors for Various Types of Materials (*6*).

Type of Material	Loss of Support
Cement-treated granular base (E = $1x10^6$ to $2x10^6$ psi)	0.0 to 1.0
Cement aggregate mixtures (E = 500,000 to $1x10^6$ psi)	0.0 to 1.0
Asphalt-treated bases (E = 350,000 to $1x10^6$ psi)	0.0 to 1.0
Bituminous-stabilized mixture (E = 40,000 to 300,000 psi)	0.0 to 1.0
Lime-stabilized materials (E = 20,000 to 70,000 psi)	1.0 to 3.0
Unbound granular materials (E = 15,000 to 45,000 psi)	1.0 to 3.0
Fine-grained or natural subgrade materials (E = 3,000 to 40,000 psi)	2.0 to 3.0

MECHANISTIC-EMPIRICAL PAVEMENT DESIGN GUIDE (MEPDG)

The MEPDG addresses erosion through modeling faulting distress (Equations 6 and 7). Classes of erodibility are formulated based on a modification of Permanent International Association of Road Congresses (PIARC) specifications relative to material type and stabilizer percent. Five levels of erosion resistance listed in Table 5, distinguish between material types based on stabilizer type and content (asphalt or portland cement) as well as long-term compressive strength (later than 28 days). Prediction of erodibility is closely associated with the material compressive strength and is readily available in most databases.

Moreover, the presence of permeable drainage layer (treated or untreated granular material with permeability > 300 ft/day) and/or a geotextile fabric between the treated base and subgrade are design features to enhance design. Each class of erosion is assumed to offer five times the resistance to erosion than the next class (i.e., Class 1 materials are five times more erosion resistant than Class 2 and so on). However, guidelines do not address the degree of friction between the concrete and the base layer or its contribution to erosion of interface via shear stress. Field performance has been

good even though lower strength materials have been used with low friction interface bases.

$$FAULTMAX_i = FAULTMAX_0 + C_7 * \sum_{j=1}^{m} DE_j * Log(1 + C_5 * 5.0^{EROD})^{C_6} \quad \textbf{(6)}$$

$$FAULTMAX_0 = C_{12} * \delta_{curling} * \left[Log(1 + C_5 * 5.0^{EROD}) * Log(\frac{P_{200} * WetDays}{P_s}) \right]^{C_6} \quad \textbf{(7)}$$

where: $FAULTMAX_i$ = maximum mean transverse joint faulting for month i, in

$FAULTMAX_0$ = initial maximum mean transverse joint faulting, in

$EROD$ = base/subbase erodibility factor

DE_i = differential deformation energy accumulated during month i

$EROD$ = base/subbase erodibility factor

C_{12} = $C_1 + C_2 * FR^{0.25}$

C_i = calibration constants

FR = base freezing index defined as percentage of time the top base temperature is below freezing (32 °F) temperature

$\delta_{curling}$ = maximum mean monthly slab corner upward deflection PCC due to temperature curling and moisture warping

P_s = overburden on subgrade, lb

$P200$ = percent subgrade material passing #200 sieve

$WetDays$ = average annual number of wet days (greater than 0.1 in rainfall)

Table 5. MEPDG Recommendations for Assessing Erosion Potential of Base Material *(7)*.

Erodibility Class	Material Description and Testing
1	(a) Lean concrete with approximately 8 percent cement; or with long-term compressive strength > 2500 psi (>2000 psi at 28 days) and a granular subbase layer or a stabilized soil layer, or a geotextile fabric is placed between the treated base and subgrade, otherwise Class 2. (b) Hot-mixed asphalt concrete with 6 percent asphalt cement that passes appropriate stripping tests and aggregate tests and a granular subbase layer or a stabilized soil layer (otherwise Class 2). (c) Permeable drainage layer (asphalt treated aggregate or cement treated aggregate and with an appropriate granular or geotextile separation layer placed between the treated permeable base and subgrade.
2	(a) Cement-treated granular material with 5 percent cement manufactured in plant, or long-term compressive strength 2000 to 2500 psi (1500 to 2000 psi at 28 days) and a granular subbase layer or a stabilized soil layer, or a geotextile fabric is placed between the treated base and subgrade, otherwise Class 3. (b) Asphalt-treated granular material with 4 percent asphalt cement that passes appropriate stripping test and a granular subbase layer or a treated soil layer or a geotextile fabric is placed between the treated base and subgrade, otherwise Class 3.
3	(a) Cement-treated granular material with 3.5 percent cement manufactured in plant, or with long-term compressive strength 1000 to 2000 psi (750 to 1500 psi at 28 days). (b) Asphalt-treated granular material with 3 percent asphalt cement that passes appropriate stripping test.
4	Unbound crushed granular material having dense gradation and high quality aggregates.
5	Untreated soils (PCC slab placed on prepared/compacted subgrade)

CHAPTER 5
EROSION MODELS

The presence of water, the erodibility of a subbase material, the rate of water ejection, the amount of deflection, and the number of load are factors that influence erosion but current design procedures scarcely address these factors. Below are models listed in the literature to address the erosion mechanism.

MARKOWL, 1984

An empirical model (Equation 8) based on the AASHO road test data relating slab thickness to equivalent single axle load (ESAL) and subbase drainage conditions. The model is simple but does not consider many important factors. The pumping index indicates the potential of erosion that increases with cumulative number of ESAL and diminishing drainage conditions but decreases quickly with an increase in slab thickness. Drainage adjustment factor is considered based on subbase permeability (*4*).

$$P_i = m \cdot \sum ESAL \cdot f_d$$
$$\log m = 1.07 - 0.34D \qquad \textbf{(8)}$$

where: P_i = pumping index
D = slab thickness (in)
$ESAL$ = equivalent 80 kN (18,000 lb) single axle loads
f_d = drainage adjustment factor
= 0.2 for good drainage (k =10,000 ft/day)
= 0.6 for fair drainage (k = 100 ft/day)
= 1.0 for poor drainage (k = 0.1 ft/day)
k = subbase permeability

LARRALDE, 1984

Another empirical model was developed based on the AASHTO road test data relating erosion to the amounts of deformation energy imposed by the application of load. The deformation energy was computed using finite element modeling; a pumping index is normalized to eliminate the effect of slab length and reinforcement. The model in Equation 9 is empirical in nature and consequently does not consider many important factors related to erosion (*4*).

$$NPI = \exp\left[-2.884 + 1.652 \cdot \log\left(\frac{\sum ESAL \cdot DE}{10{,}000}\right)\right] \quad \textbf{(9)}$$

where: NPI = normalized pumping index of volume of pumped material (in^3)

$ESAL$ = equivalent 80 kN (18,000 lb) single axle loads

DE = deformation energy per one application of ESAL

$= \log(DE) = 3.5754 - 0.3323\,D$

D = slab thickness (in)

RAUHUT, 1982

In this model, the level of pumping damage was empirically related, based on nonlinear regression analysis of the Concrete Pavement Evaluation System (COPES) database, to many comprehensive factors such as precipitation, drainage, subbase type (stabilized or not), subgrade type (soil type), load transfer, slab thickness, freezing index, Thornthwaite moisture index, and traffic. Equation 10 is separated for jointed plain concrete pavement (JPCP) in Equations 11 and 12, and JRCP in Equations 13 and 14 (*4*).

$$g = \left(\frac{\text{ESAL}}{\rho}\right)^{\beta} \quad \textbf{(10)}$$

JPCP

$$\ln\rho = 1.39 \cdot \text{DRAIN} + 4.13 \quad \textbf{(11)}$$

$$\beta = \frac{0.772(D-2.3)^{1.61}}{PPTN} + 0.0157 \cdot JLTS \cdot D + 0.104 \cdot STAB + 0.17 \cdot DRAIN + 0.137 \cdot SOILTYP - 0.247 \quad \textbf{(12)}$$

JRCP

$$\ln\rho = 1.028 \cdot STAB + 0.0004966 \cdot D^{3.47} - 0.01248 \cdot FRINDEX + 1.667 \cdot CBR + 5.476 \quad \textbf{(13)}$$

$$\beta = -0.01363 \cdot DMOIST + 0.02527 \cdot D - 0.423 \quad \textbf{(14)}$$

where:

g	= amount of distress as a fraction of a pumping level of 3 (severe)
DRAIN	= 0; no underdrains, 1; underdrains
PPTN	= average annual precipitation (cm)
JLTS	= 0; undoweled, 1; doweled
STAB	= 0; unstabilized subbase, 1; stabilized subbase
SOILTYP	= 0; granular foundation soil, 1; coarse foundation soil
DMOIST	= Thornthwaite moisture index
FRINDEX	= freezing index
CBR	= California bearing ratio of foundation soil
D	= slab thickness (in)

VAN WIJK, 1985

Equations 15 and 16 included factors derived from field data to make improvement over the Larralde model to predict the volume of eroded material as a function of the deformation energy produced by traffic. The effect of many factors on pumping such as subbase and subgrade type, drainage, load transfer, and climate condition are considered in this model. Since this model is empirical in nature, its application is limited to the variable ranges included in the database (*4*).

$$P = 36.67 \cdot NPI \quad \textbf{(15)}$$

$$NPI = F \cdot \exp\left[-2.884 + 1.652 \cdot \log\left(\frac{\sum ESAL \cdot DE}{10{,}000}\right)\right] \quad \textbf{(16)}$$

where: P = volume of pumped material (ft^3/mile)

NPI = normalized pumping index (in^3)

DE = deformation energy per application (in-lb)

$\log(DE) = 3.5754 - 0.3323\,D$

D = slab thickness (in)

F = f_{JPCP} if nonreinforced PCC, f_{JRCP} if reinforced PCC

P = volume of pumped material (ft^3/mile)

$f_{JPCP} = f_{sbl} \cdot f_d \cdot f_{lt} \cdot f_{prec} \cdot f_{sg}$

f_{sbl} = subbase adjustment factor: 1; unstabilized

0.65+0.18 log(ΣESAL); stabilized

f_d = drainage adjustment factor: 1; poor drainage

0.91+0.12 log(ΣESAL)-0.03D; fair drainage

0.68+0.15 log(ΣESAL)-0.04D; good drainage

0.01; excellent drainage

f_{lt} = load transfer adequacy adjustment factor: 1; with dowel

1.17-0.68 log(ΣESAL)-0.078D; without dowel

f_{prec} = rainfall adjustment factor:

0.89+0.26 log(ΣESAL)-0.07D; dry climates

0.96+0.06 log(ΣESAL)+0.02D; wet climates

f_{sg} = subgrade adjustment factor: 1; granular subgrades

0.57+0.21 log(ΣESAL); coarse subgrade

$f_{JRCP} = f_{sb2} \cdot f_e$

f_{sb2} = subbase adjustment factor: 1; unstabilized

0.91-0.02 log(ΣESAL); stabilized

f_e = adjustment for climate:

0.011+0.003 log(ΣESAL)-0.001D; dry, warm climates

1.44-0.03 log(ΣESAL)-0.06D; wet, warm climates

1.04-0.32 log(ΣESAL)-0.08D; dry, cold climates

0.54-0.85 log(ΣESAL)-0.19D; wet, cold climates

JEONG AND ZOLLINGER, 2003

A mechanistic empirical model (Equation 17) was developed using the water-induced shear stresses model proposed by Van Wijk (*4*). Key factors such as vehicle load and speed, load transfer, number of applications, and climatic conditions are included in the model to predict erosion. Erosion potential increases with higher initial edge gap and liftoff distance due to the effect of upward curling along slab corners and edges inducing shear stress on the base layer by pumping of trapped water. The magnitude of shear stress depends on the dynamic viscosity of water governed by water temperature and the speed of slab deflection. Higher slab deflection velocity and lower viscosity of water result in more erosion of the base while better load transfer cuts down erosion rate as detailed in the performance equation. The accuracy of the model should be calibrated using performance data such as that may be available in the Long-Term Pavement Performance (LTPP) database (*8*). This model can be improved through consideration of abrasive erosion by friction between concrete and subbase layer.

$$v = v_0 e^{-\left(\frac{\rho}{N_i}\right)^a} \quad \textbf{(17)}$$

where: v_0 = ultimate erosion depth (L)

N = number of axle loads per load group

ρ = calibration coefficient based on local performance

a = $a' \alpha_f$

a' = environmental calibration coefficient

α_f = inverse of the rate of void development

$$= \left[\frac{\partial v_i}{\partial t}\right]^{-1} = \left[\frac{Log^{-1}(a_m \tau + b_m)}{\gamma_b}\right]^{-1} = \left[\frac{\beta}{\gamma_b}\right]^{-1}$$

τ = shear stress = $\frac{\eta B}{\delta_{void}}\left(1 - \frac{LTE}{100}\right)$

η = dynamic viscosity of water ($FL^{-2}t$)

$= \left\{2056.82 + 10.56T - 284.93\sqrt{T} - 265.02e^{-T}\right\}10^{-6}$

T = water temperature (°C)

$B = V_{z_i} \sin\theta + 6V_{z_i}\left[\frac{\sin\theta}{2} + \frac{\cos^2\theta}{\sin\theta}\right]$ (L/t)

δ_{void} = void space below slab for water movement

θ = slab angle = $\tan^{-1}\left[\frac{z_o}{s}\right]$

z_o = edge gap (L) = $\frac{(1+\nu)}{H}\Delta\varepsilon_{tot}\ell^2$

$V_{z_i} = \frac{\delta_{\text{int}}}{s \diagup V_i}$

$\delta_{\text{int}} = \frac{P_i}{8k\ell}\left\{1 + \left[0.3665\log\left(\frac{a_L}{\ell}\right) - 0.2174\left(\frac{a_L}{\ell}\right)^2\right]\right\}$

a_L = loaded radius (L)

P_i = axle load (F)

s = slab liftoff distance (L) = $\sqrt{2}\ell(\gamma - 1)$

$\gamma = \sqrt{\frac{z_o}{w_o}}$

$w_o = \frac{\rho H}{k}$

CHAPTER 6
LABORATORY TEST METHODS FOR EROSION

Many erosion tests were developed in 1970s and 1980s using various testing devices but none of those tests have been selected as standard test method. The following test methods are reviewed and evaluated relative to their utility to characterize subbase and subgrade materials for erosion resistance.

ROTATIONAL SHEAR DEVICE AND JETTING DEVICE—VAN WIJK, 1985

Figure 35 shows the testing devices developed to measure erosion using pressurized water. The concept is based on surface erosion occurring when water-induced shear stress is higher than the shear strength of test material. Two different devices are used depending upon the cohesive nature of the tested material. Cohesive materials are tested using a rotational shear device, while noncohesive materials are tested using a jetting device. Both methods consider only hydraulically induced shear on erosion process. Weight loss could be overestimated by the loss of aggregate-sized particles, which may not take place in the field.

Rotational Shear Device

Erosion occurs by rotating water around cohesive specimen to determine the shear strength for each material. Due to the ease of adjustment of the shear force, a wide range of subbase materials can be tested. Nonhydraulic erosion is not considered in this test.

Jetting Device

The jetting device test equipment ejects pressurized water at an angle of approximately 20 degrees to the upper surface of noncohesive samples generating weight loss over time. Shear stress determinations on the surface are calculated based on the assumption of stress being placed over a uniform area even though the surface area changes with time and surface pressure distribution.

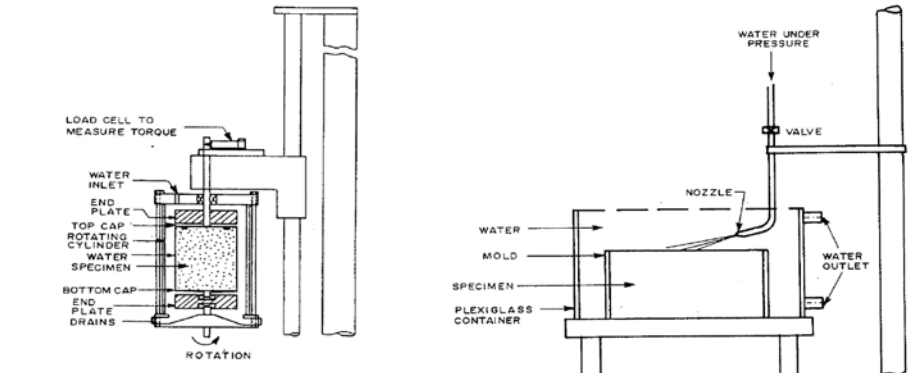

Rotational Shear Device Jetting Device

Figure 35. Rotational Shear Device and Jetting Device (*4*).

BRUSH TEST DEVICE—PHU ET AL., 1979

Figure 36 shows details of the brush test used by French researchers, allowing various material types to be characterized by an erosion index, IE (*5*). Various masses are applied to the linear brush test, while one kg is used for the rotational brush test. IE is defined as the ratio of the weight loss to that of a granular material stabilized with 3.5 percent cement (reference material); 26 g/min is regarded as one unit of IE. Lower IE means better erosion resistance. A table of various material types was suggested as a design guide for erosion (Figure 37). The major drawback is the long test time involved (6 weeks for wet-dry durability brush tests). Although a common issue with all erosion tests, base materials consisting of large-sized aggregates that loosen and dislodge during testing create inaccurate weight loss data.

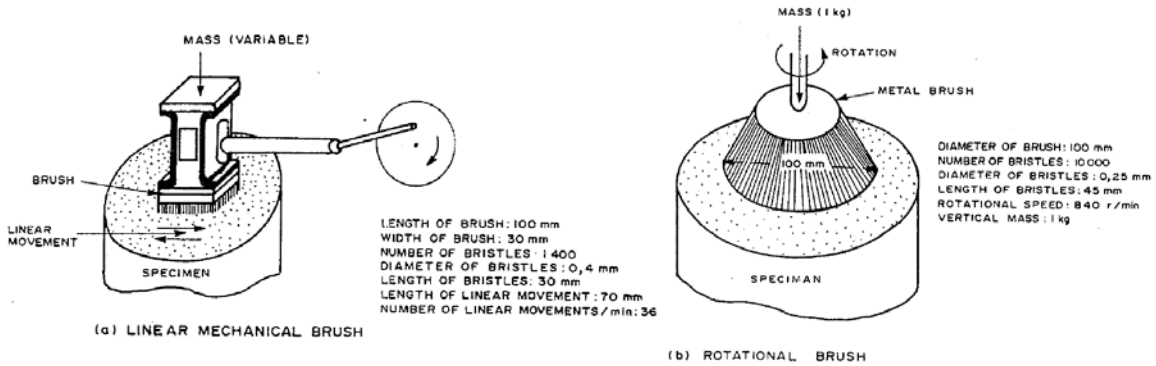

Figure 36. Brush Test Devices (*5*).

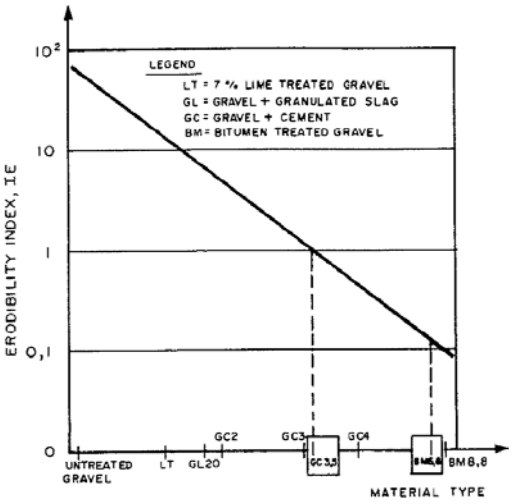

TABLE : DETAIL OF MATERIALS

MATERIALS		STABILIZER (%)	AVERAGE ERODIBILITY (g/min)	ERODIBILITY INDEX, IE
BITUMEN TREATED GRAVEL	BM 2,2	2,2	57	2,19
	BM 4,4	4,4	10	0,38
	BM 6,6	6,6	6	0,23
	BM 8,8	8,8	3	0,10
GRAVEL + CEMENT	GC 2,2	2,0	132	5,00
	GC 3	3,0	30	1,15
	GC 3,5	3,5	26	,00
	GC 4	4,0	12	0,46
	GC 6	6,0	10	0,38
	GC 9	9,0	8	0,30
GRAVEL + GRANULATED SLAG	GL 20/40	20	168	6,46
	GL 40/60	20	193	7,42
LIME TREATED GRAVEL	LT	7	350	13,50
UNTREATED GRAVEL	GNT		1 231	47,00

Figure 37. Proposed Erodibility Index (*5*).

ROLLING WHEEL EROSION TEST DEVICE—M. DE BEER, 1989

Figure 38 shows an empirical test procedure for erosion proposed in South Africa several years ago (*9*). Wheel movement over a friction pad serves as the source of erosion of the test sample. Fines are produced on the surface of the test sample by direct contact between the friction pad (neoprene membrane) and the test sample; submerging the test sample during testing allows water to wash out generated fines similar as would take place under pumping action. The erosion index is the measure of erosion and defined as the average depth of erosion after 5000 wheel load applications. The test method evaluates the erodibility based on the depth of erosion rather than the weight loss of the sample.

This test attempts to simulate field conditions since it addresses mechanical abrasive and hydraulic erosion together. However, pumping action caused by the flexible membrane in this test may not be similar to the pumping action under rigid pavement; nether is the applied shear stress under this method easily discernable. The voiding of the base material due to erosion would be difficult to represent in this test configuration. The other factor that could affect the erodibility of this test is the surface condition of the sample. When preparing the test sample, the testing surface is cut by a saw blade. Accordingly, this sample preparation could generate surface damage causing artificially high weight loss.

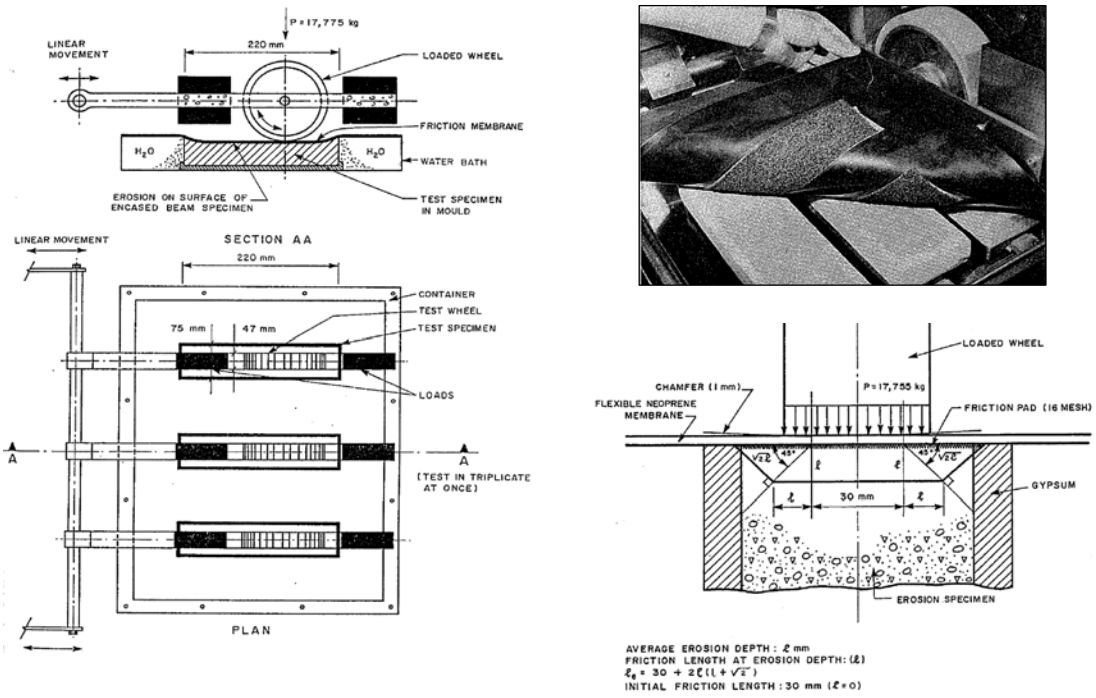

Figure 38. Rolling Wheel Erosion Test Device (*9*).

CHAPTER 7
ERODIBILITY OF ALTERNATIVE SUBBASE MATERIALS

A list of alternative subbase types and materials was developed based on evaluation of field performance and discussion with the project monitoring committee. Accordingly, cement-treated bases are at the top of the list as they are performing well in many instances. Recyclable materials (recycled asphalt and recycled concrete) also show promise and are the focus of current laboratory testing. Combinations of selected recycled materials are part of an ongoing test program and test results to date are summarized as well as a discussion of the test procedures.

LIST OF ALTERNATIVE SUBBASE MATERIALS

The features of an ideal subbase layer might consist of sufficient strength having at moderate level at friction, erosion resistance, and a conforming but uniform support. A subbase layer should be adequately flexible to minimize curling and warping-related stress as well as reflection cracking in the concrete slab. Additionally, a medium level of frictional restraint (avoiding any interlocking with the slab) is desired to minimize the shear stress between the concrete and the base layer.

With these suggested features, a variety of candidate subbase types are listed in Table 6 and can be evaluated in terms of the desirable features of an ideal subbase layer.

Each alternative subbase material in the list is evaluated relative to the performance factors listed in the heading of Table 7.

Table 6. Features of Candidate Alternative Subbase Types.

Type	Stabilize Agent or Interlayer	Aggregate Type	Combination Features	Specification Items
Cement-treated base	Cement	Limestone or gravel	Cement + flex base	Item 275
Reclaimed asphalt pavement (RAP) base	Cement and RAP	Crushed asphalt and limestone/ gravel	Cement + RAP > 50% subbase	Item 305, 275
Recycled concrete base	Cement	Crushed concrete	Cement + 100% crushed concrete	Item 251, 275
Lime-fly ash treated base	Lime or fly ash	Limestone or gravel	Lime and/or fly ash + flex base	Item 260, 265
Thin AC on treated subgrade	Lime or cement depending on soil type	Subgrade material	2 in AC base over treated subgrade (usually 8 in min)	Item 330, 275
Recycled Asphalt Pavement (RAP)/AC bond breaker	RAP asphalt	Limestone or gravel	RAP > 30% bond breaker over CTB	Item 305, 275
Emulsion bond breaker	Emulsion	Limestone or gravel	Emulsion bond breaker over CTB	Item 300, 275

Table 7. Performance Comparisons of Candidate Alternative Subbase Types.

Type	Stabilizer Content	Coefficient of Friction (when natural subgrade = 1)	Elastic Modulus, ksi (*6*)	Erosion Ratio, g/min (*5*)	Relative Cost to 4 in AC Bond Breaker
Cement-treated base	3% cement	10	1,000 ~ 2,000	30	Low
RAP base	2-4% cement	6	350 ~ 1,000	57	Low
Recycled concrete base	3% cement + 1% residuals	15	450 ~ 1,500	12	Low
Lime-fly ash treated base	1:3 lime/fly ash	10	20 ~ 70	350	Low
Thin AC on treated subgrade	cement or lime	6	350 ~ 1,000	AC:10, CTS:* 132	Medium
RAP/AC bond breaker	4.4% asphalt concrete	6	350 ~ 1,000	AC:10, CTB:** 30	Medium
Emulsion bond breaker	3% cement	3	CTB**: 1,000 ~ 2,000	Emulsion: N/A CTB:** 30	Medium

* CTS - Cement-Treated Subgrade **CTB – Cement-Treated Base

TxDOT subbase design practice calls for either a 6 in CTB with a 1 in AC bond breaker or a 4 in AC layer over a treated subgrade. Using a reduced thickness or high RAP content AC layer may be a possibility to reduce cost. Using a spray-on emulsion (asphalt, resin, or wax-based emulsions) may have certain advantages particularly from a construction perspective, but this option would be limited to stiff concrete subbases in order to ensure nonerodibility. The purpose of the emulsion would be to reduce the interlayer friction to acceptable levels but maintain a certain amount of bond. Perhaps, the use of asphalt cement in this manner would be a more economical means to providing a debonding effect between the slab and the subbase.

Considering these characteristics in light of the objective of identifying alternative subbase types and materials, CTB or cement stabilized base (CSB), RAP, and the subbase materials using recycled concrete are selected as some of the most feasible candidate alternative subbase combinations.

Cement-Treated Base

CTB has been widely used along with an AC bond breaker under concrete pavements for many years in Texas. The bond breaker has been used to improve the action of the reinforcing steel to achieve suitable cracking patterns in CRC pavement. In order to utilize CTB subbase, some measures are required to keep friction levels to tolerable limits. Apparently, there may be some evidence to suggest the effect of a bond breaker upon the crack pattern of CRC pavement is minimal. However, CTBs yielding this type of performance may also be susceptible to a high rate of erosion.

Advantages

The advantage of a CTB is the higher material strength and stiffness and resistance to erosion. A CTB layer is also practically impervious and insensitive to the cyclic damage of freezing and thaw; moreover, it gains strength with age (*10*).

Disadvantages

CTB may have a tendency to reflect cracking through the surface layer; this is rarely an issue with CRC pavement. The main disadvantage with a CTB layer is the need to balance erodibility against layer stiffness and interlayer friction. A consequence of not maintaining this balance is the need to use a bond breaker to prevent erosion damage.

Reclaimed Asphalt Pavement Base

RAP is the removed and/or reprocessed asphalt materials and aggregates for pavement reconstruction. Full-depth reclamation uses a mix of the base material and the deteriorated asphalt pavement with the addition of cement to create a new stabilized base material. Recycling costs are less than the removal and replacement of the old pavement and performance has been satisfactory relative to the original subbase (*10*, *11*).

Advantages

RAP has economical and environmental benefits since its use potentially saves material, energy, and disposal costs, as well as conserving natural resources. RAP also has good availability for construction since it typically can be obtained, processed, and used onsite. RAP may also provide low friction between the concrete slab and the subbase layer (*10*).

Disadvantages

The quality of RAP is highly governed by constituent materials and there can be substantial variation in aggregate quality, size, and consistency depending on the source of the original material. Moreover, milling and crushing during processing can cause aggregate degradation and the amount of fines generated. This variation can cause reduction in subbase stiffness and strength possibly creating low erosion resistance (*11*).

Recycled Concrete Base (RCB)

Recycled concrete pavement has become an important candidate as an alternative subbase material due to less erosion potential with high durability as well as being economically and environmentally feasible. Lab testing should be useful to evaluate

erodibility and brittleness versus various cement contents; previous research recommended only 1.5 percent cement content as optimal for stabilizing based on unconfined compressive strength, durability, and moisture susceptibility testing (*12*). Such low cement content may be the result of the residual cementitious material on the surface of the crushed concrete.

Advantages

Similar as RAP, the use of recycled concrete may have many economical and environmental advantages such as a lower haul distance, reduced usage of natural aggregates, and lower energy consumption and waste. Previous research has found that recycled concrete materials cause CTB mixtures to set quicker with slightly higher (about 2 percent) density than mixtures with conventional aggregates as well as higher long-term strength (*13*).

Disadvantages

Benefits using RCB could only be realized where sufficient quantities of recycled concrete material are available near the construction site. RCB may segregate when worked excessively during compaction (*14*).

EROSION TEST RESULTS

The laboratory test program underway involves measuring the erodibility of different subbase materials. The new test configuration shown in Figure 39 consists of two component layers—one being concrete and the other the material of interest consisting of either 1) cement-treated base, 2) RAP base, and 3) 100 percent recycled crushed concrete base as candidate economical erosion resistant subbase materials. The tests were conducted with a tri-axial type device where the load levels of σ_1 and σ_2 were controlled to provide a cyclic deviatory stress at specified levels (creating various shear stress levels). This configuration provides mechanical abrasion under a 100 psi normal stress where weight loss occurs due to friction restraint. The following three characters are determined from the test results:

- critical shear strength of material at the interface based on a static loading test,
- friction factors (coefficient of friction) at normal and critical levels of shear stress, and
- weight loss rate at different shear stress levels.

Because of the inherent stiffness associated with this configuration some interpretation of the test results is necessary for application to pavement layer configurations based on composite deformation within each layer and interfacial friction. This is accomplished using multilayer analysis to relate the load-induced shear stresses in the test to the shear stresses under field conditions. Partial test results are summarized since additional testing is in progress.

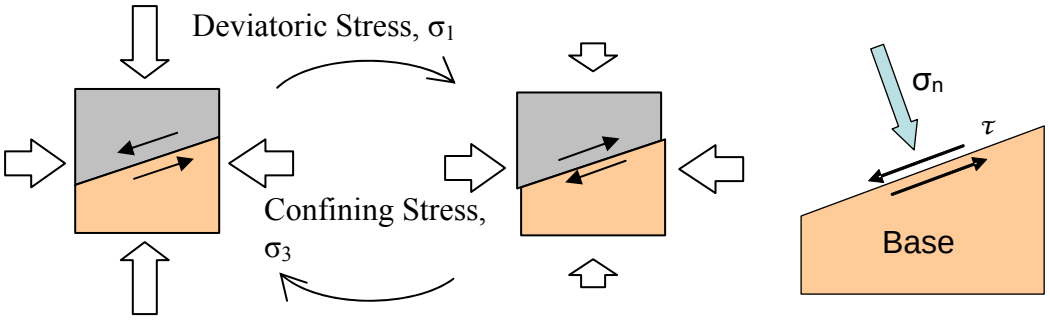

Figure 39. Erosion Test using Tri-axial Device.

Sample Preparation

The following four different sample types are selected for erosion testing. All samples are stabilized using 3 percent cement and optimum moisture content plus 0.75 percent water by weight:

1. CTB sample–limestone base material from Bryan District;
2. 30 percent RAP sample–30 percent RAP + base material (shell/dark soil) from Beaumont District;

3. 50 percent RAP sample–50 percent RAP + base material (shell/sandy soil) from Beaumont District; and
4. RCB sample–Recycled crushed concrete.

Material gradation of the base materials are shown in Figure 40. The CTB and RCB gradations meet the requirements of American Society of Testing Materials (ASTM) D 2940-03 but the RAP material contains more fines (less than 4.75 mm or No. 4 sieve size).

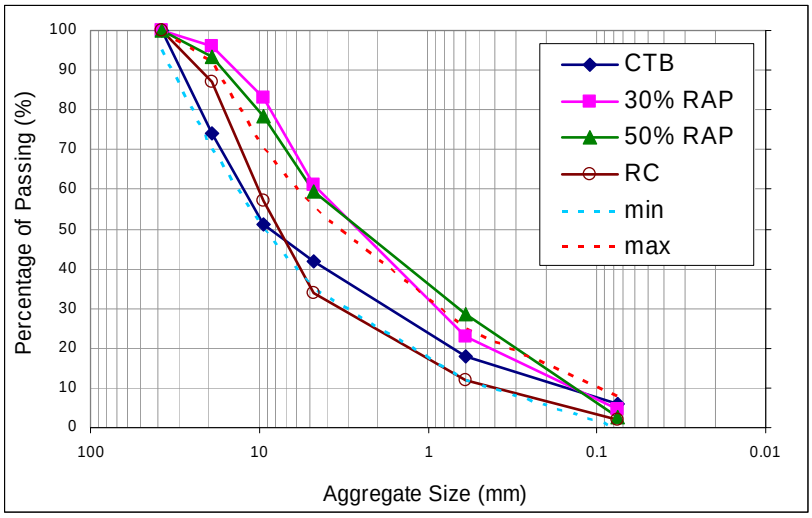

Figure 40. Aggregate Size Distributions of Samples.

All samples were prepared according to the test method "Tex-120-E, Soil-Cement Testing" and compacted according to the test method "Tex-113-E, Laboratory Compaction Characteristics and Moisture-density Relationship of Base Materials," using a 10 lb hammer, with an 18 in drop, at 50 blows/layer in a 6 x 8 in mold. All samples were cured more than 90 days under 100 percent relative humidity conditions. All samples were cut on a 40-degree slant. Special precautions were taken to prevent edge damage during cutting and testing. Figure 41 shows sample surface conditions where the CTB sample shows the relatively larger size of aggregates on the surface.

CTB

30% RAP

50% RAP

RCB

Figure 41 Surface Condition of Samples.

Erosion Test Result

The erosion of stabilized materials is highly dependent upon the strength of the cementitious matrix and the durability of the aggregate. Since bound materials may have cohesive strength, the applied shear stress may not be sufficient to generate shear failure in the surface material. Shear stress induced by surface friction may erode the interface of concrete and base/subbase. Figure 42 shows a test specimen configuration where the 40-degree angled concrete block is cycled against the base material under a load of 100 psi applied normally and at various levels of shear stresses by changing deviatoric stress and confining stress. Other angles were experimented with but were not able to generate

sufficient abrasion to wear away material at the interface. Weight loss was measured at five different levels of shear stress at the interface. Loading time was 0.2 s sinusoidal pulse loading and 0.8 s rest period per every second to simulate vehicle loading on concrete pavement.

Figure 42. Configuration of Test Sample.

Figure 43 shows weight loss after 1000 load repetitions under various shear stress levels. As expected, more weight loss develops as shear stress increases. However, the rate of weight loss dropped off to some extent at higher stress levels. RAP base samples experienced a greater weight loss than the RCB because of a greater fines content. However, the 30 percent RAP base experienced more weight loss than the 50 percent RAP base because a lower RAP content resulted in a less durable combination. Interestingly, the CTB eroded less than the RCB at a high level of shear stress even though the gradation was finer than the CTB. It is clear the exposed aggregate affects the rate of erosion and the results should be normalized accordingly.

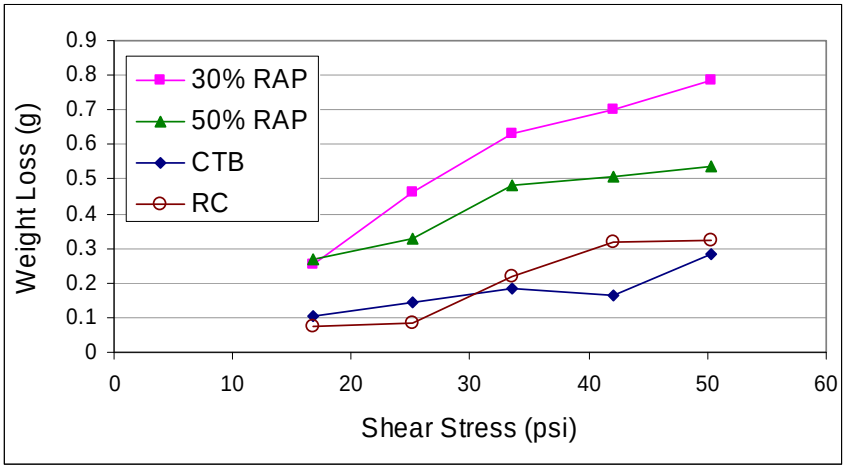

Figure 43. Weight Loss versus Various Shear Stress.

Figure 44 shows the effect of the number of loading with the shear stress of 33.6 psi. Weight loss increased with loading repetition but the rate again diminished after 3000 repetitions. The one possible reason is the amount of generated fines causes a reduction in shear stress at the interface of two layers. To minimize the effect of the accumulated fines on the induced shear stress, periodically cleaning of the interface is conducted as such would take place under pumping action. The spikes in the results (CTB and 30 percent RAP 3000 repetition and RC 5000 repetition) are caused by removal of relatively large-sized aggregate in the mixture relative to other generated fines.

Based on the test results, abrasive erosion is governed by gradation and aggregate content of the base. Therefore, a more uniform rate of erodibility may be achieved through samples without coarse aggregates larger than 4.75 mm (#4 sieve size).

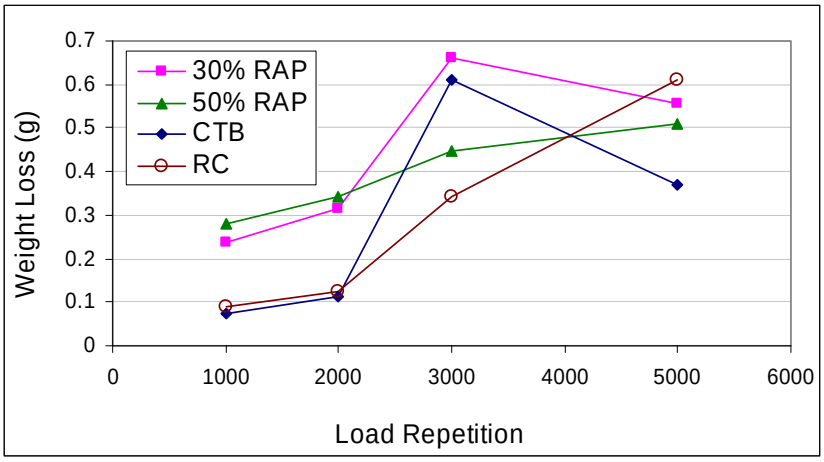

Figure 44. Weight Loss versus Various Number of Loading.

CHAPTER 8
CONCRETE SLAB BEHAVIOR AND MODULUS OF SUBGRADE REACTION

The characterization of subgrade materials under concrete pavement systems, since the inception of Westergaard's analysis, has been based upon dense liquid behavior. The basic characteristic of a dense liquid or Winkler subgrade is a spring constant referred to as a k-value. Researchers note that although the Westergaard solution agreed fairly well with their observations for interior loading conditions, it failed to give even a close estimate of the response for edge and corner loads. Nonetheless, the most accepted subgrade characterization for concrete pavement design is the Winkler foundation since the Winkler foundation is an easy model to understand and to apply to the design process.

It should be pointed out that k-value is not an intrinsic property of the soil or the supporting medium which consequently has led to difficulties of consistency in the evaluation of soil strength and stiffness using different testing procedures and methodologies. On the other end of the subgrade idealization spectrum, due to its ease of determination in the laboratory, there has been a great deal of interest in using the elastic modulus of the soil for design rather than the soil k-value, which means making use of a correlation between k-value and the soil elastic modulus so that the result from a resilient modulus test in the lab could be substituted into the Westergaard design analysis.

Although a k-subgrade may only be behaviorally remotely associated with the behavior of an elastic subgrade (E_s, which has units of force/unit area), correlations between k-value and subgrade modulus have been drawn in various forms and degrees in many of the past versions of the AASHTO Design Guide. In reality, such correlations are complicated due to the necessity for the development of an equivalence between these vastly different subgrade theories (k-value versus an elastic modulus) even when it is limited to interior portions of a concrete slab. Either of these theories can be used to predict subgrade stress, subgrade deflection, or slab bending stress of a loaded pavement slab. However, as previously noted, the establishment of a correlation between k-value and E_s requires the assumption that one of the three above pavement responses are equal

between the two theories—with the problem being that either one of the equivalencies will yield a different answer as to what that correlation should be.

In order to avoid the limitations associated with such correlations, it is recommended to focus the characterization of the subgrade support on material properties or parameters that directly correlate to the subgrade model at hand and not determine a material characteristic relative to one model and substitute an interpretation of it into another model for use in design.

CONVERSION BETWEEN ELASTIC MODULUS AND SUBGRADE K-VALUE

Subgrade and subbase support is considered in the structural model for pavement design by the modulus of subgrade reaction, *k* (rather than the resilient modulus M_R.) Therefore, M_R measured directly from the laboratory or obtained through the use of correlations with other material strength properties needs to be converted to *k*. The MEPDG transforms the actual pavement structure into an equivalent structure with "effective" dynamic k-value to substitute for the compressibility of all layers as shown in Figure 45 (*15*).

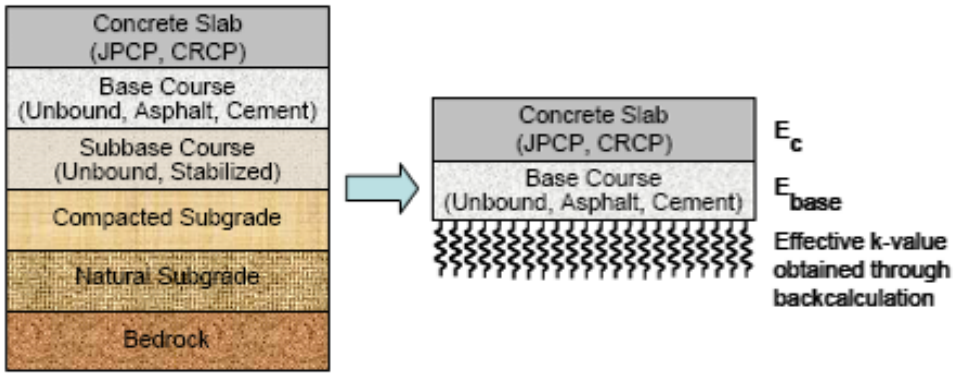

Figure 45. Structural Model for Rigid Pavement Structural Response Computations (*15*).

The procedure of computing effective dynamic k-value in the MEPDG is as follows (*15*):

1. *Assign layer parameters (E and Poisson's ratio) in a manner consistent with flexible pavement design (PART 3, Chapter 3).*
2. *Using the elastic layer program JULEA, simulate a 9000-lb Falling Weight Deflectometer (FWD) load with the plate radius 5.9 in and compute PCC surface deflections at 0, 8, 12, 18, 24, 36, and 60 in from the center of the load plate.*
3. *Adjust the subgrade resilient modulus to account for the lowered deviator stress level beneath a PCC slab and base.*
4. *Using the elastic layer program JULEA, again simulate a 9000-lb FWD load with the plate radius equal to 5.9 in; and with the recalculated subgrade resilient modulus and subbase moduli.*
5. *Calculate PCC surface deflections at 0, 8, 12, 18, 24, 36, and 60 in from the center of the load plate.*
6. *Use the Best Fit method to compute the dynamic modulus of subgrade reaction using the PCC surface deflections.*

Since there is no detailed explanation as to how the effective dynamic k-value is calculated and how it converted to a static k-value, it is difficult to evaluate the effectiveness of this procedure. However, the deflection calculated by the JULEA program may result in significantly higher dynamic k-values particularly if a full bond between two layers is utilized in its determination.

SUBGRADE K-VALUE ANALYSIS FOR RIGID PAVEMENT DESIGN

The effect of a stabilized layer in a rigid pavement design is illustrated through analyzing bending stresses and deflections using the ISLAB 2000 program. Table 8 contains the data inputs used in the analysis; Figures 46 shows the maximum stresses in the PCC slab due to an interior loading condition. The unbonded condition and lower subbase modulus resulted in higher stresses due to higher deflections. The maximum stresses in the PCC slab decrease when the subbase thickness increases; also, the stress level in the bonded condition is lower than the unbonded condition since the PCC and subbase layer behave together in a bonded condition. Also, the deflection decreases as the subbase thickness increases.

Table 8. Analysis Conditions of ISLAB 2000 Program.

PCC Slab Thickness	8 in	Poisson ratio	0.15
k-value	200 psi/in	Axle load	18,000 lb
a	6.180 in	Tire pressure	75 psi

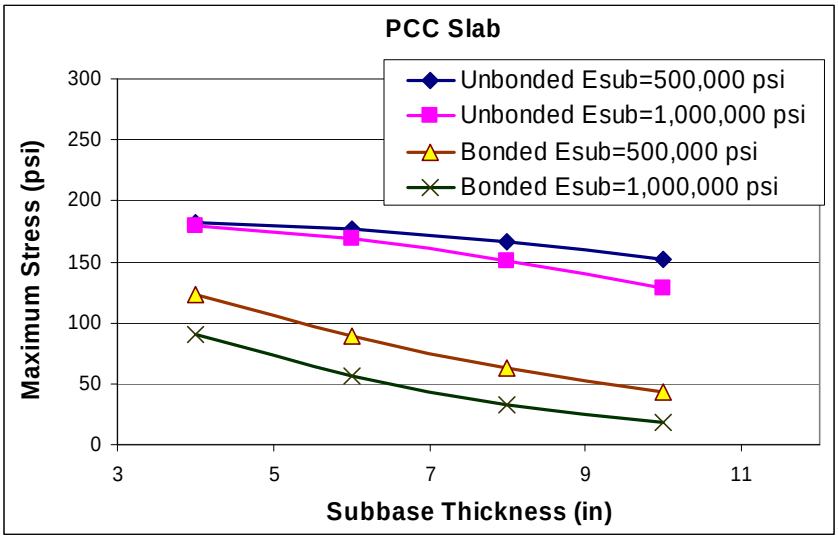

Figure 46. Maximum Stress at the Bottom of PCC Slab.

Figure 47 shows the maximum stresses at the bottom of a CTB subbase. The unbonded condition has a higher stress level than the bonded condition; the stress level in the subbase layer also increases as the subbase thickness increases in the unbonded condition. However, the stress level decreases with increasing subbase thickness in the bonded condition. The difference between the unbonded and bonded subbase behavior is reflected in the differences between the bonded and unbonded bending stresses and deflections.

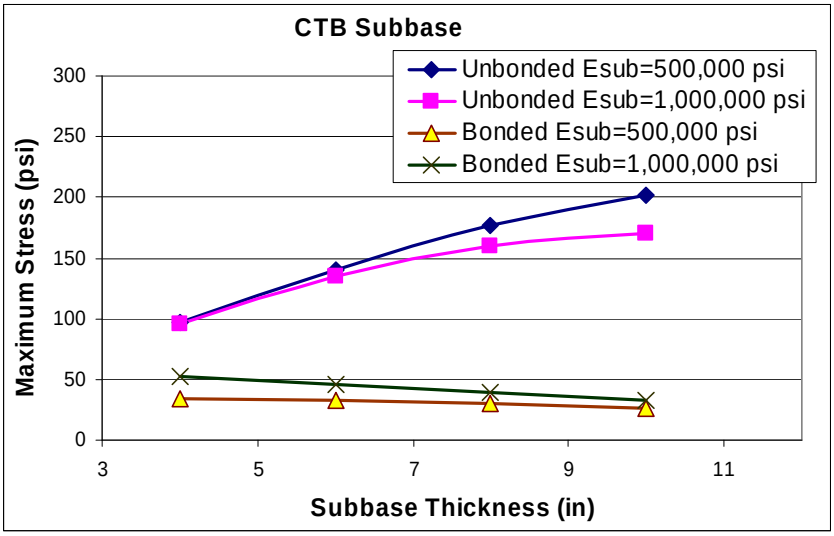

Figure 47. Maximum Stress at the Bottom of Subbase Layer.

Figure 48 shows the maximum interior deflection of a concrete slab over a CTB subbase. The deflection decreases as the subbase thickness increases; the unbonded condition shows a higher deflection than the bonded condition. As mentioned earlier, the bonded condition shows a higher rate of deflection reduction since the PCC and subbase behave as one composite layer.

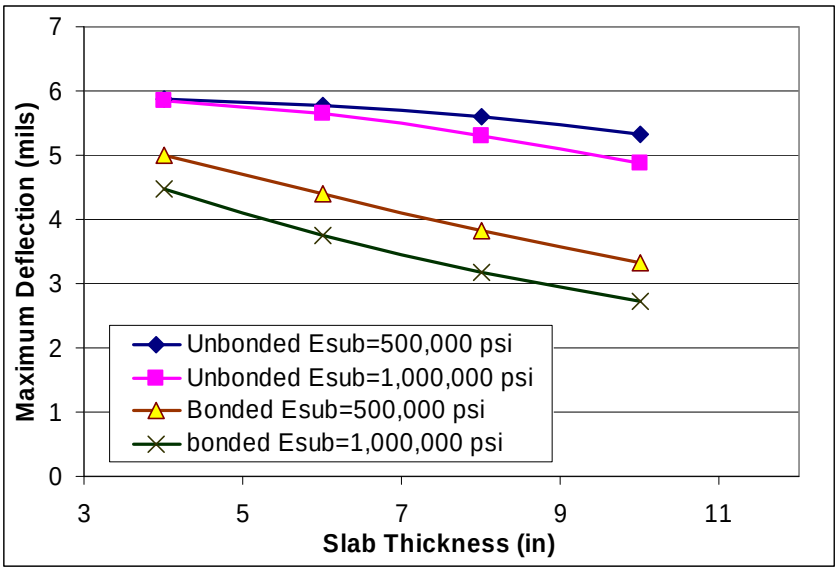

Figure 48. Maximum Deflection.

Table 9 and Figure 49 show the maximum stress and deflection of a concrete slab without a subbase. The stress and deflection decrease exponentially as k-value increases; the regression equation in Figure 49 can be used to find the equivalent k-value of a one-layer system (instead of a two-layer system with a subbase). The equivalent deflection is used to transform between the multilayer condition and the single layer condition (similar as used in the MEPDG).

Figure 50 shows the equivalent k-values based on the equivalent deflection using the equations in Figure 49. The effective k-value is significantly different between the unbonded and bonded condition; the gap becomes larger with subbase thickness. When the subbase is considered as a fully bonded layer with the PCC slab, the deflection decreases significantly and equivalent k-value for the same deflection is unrealistically high. Since partial bonding would be present in a real pavement due to subbase friction, more realistic k-values could be calculated if the friction between the slab and subbase is taken into account in the elastic modulus conversion to effective k-value.

Table 9. Maximum Stress and Deflection vs. k-values of One-Layer System.

Subgrade k-value, psi/in	Concrete Slab Stress, psi	Deflection, mils
50	212.5	12.27
100	198.5	8.49
200	185.1	5.92
300	177.3	4.81
400	171.8	4.15
500	167.6	3.704
600	164.1	3.374
700	161.1	3.117
800	158.6	2.91
900	156.3	2.739

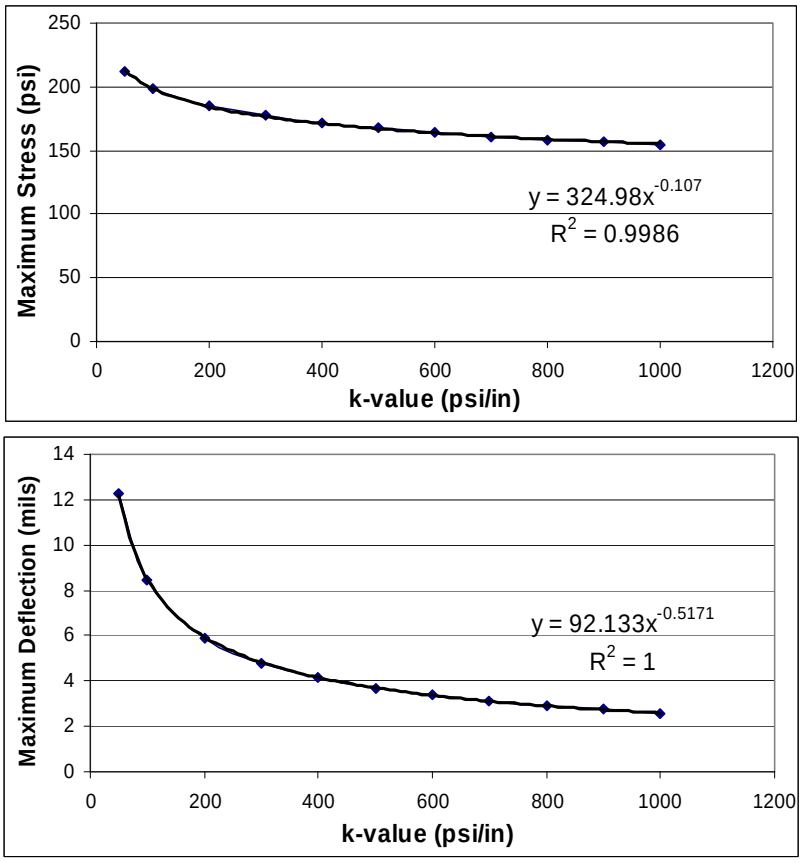

Figure 49. Maximum Stress and Deflection of One-Layer System.

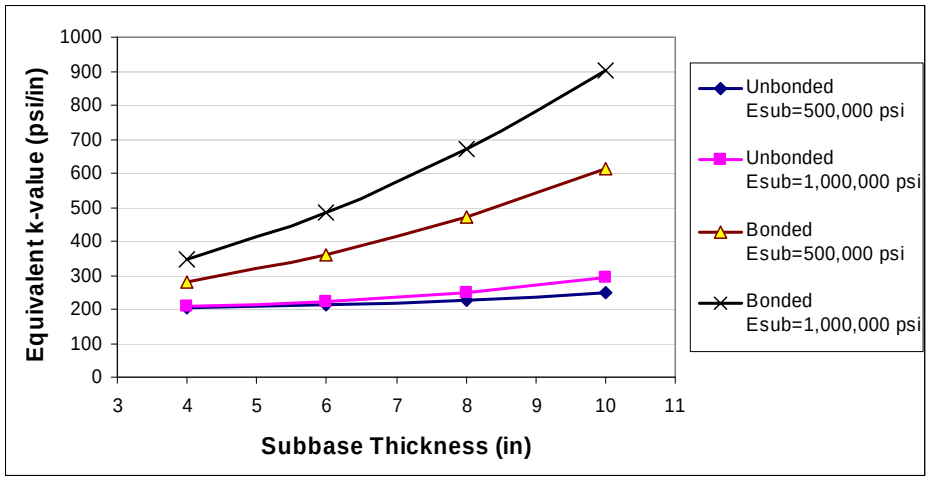

Figure 50. Equivalent k-values by Different Bonding Condition.

As an example, the combination of factors (degree of bonding, modulus, and subbase thickness) to yield k-value of 300 psi/in is examined. When the k-value is 300 psi/in in single layer condition (PCC slab directly over a 300 psi/in subgrade), the deflection of the PCC slab is 4.81 mils under 9000 lb interior loading; therefore, the combination of subbase condition factors that results in the same deflection would be the equivalent structural condition of the pavement with a subbase (using equivalent bending stress gives an unrealistic result). Table 10 shows the required subbase thickness that can result in the same deflection. Bonded and unbonded conditions show almost three times the difference for equivalent subbase thickness. Figure 51 shows deflection trends as a function of subbase thickness, modulus, and degree of bonding.

Table 10. Subbase Conditions to Correspond with the No-Subbase Case.

No.	Bonding Condition	Subbase Modulus, psi	Subbase Thickness, in
1	Unbonded	500,000	12.45
2	Unbonded	1,000,000	10.44
3	Bonded	500,000	4.63
4	Bonded	1,000,000	3.15

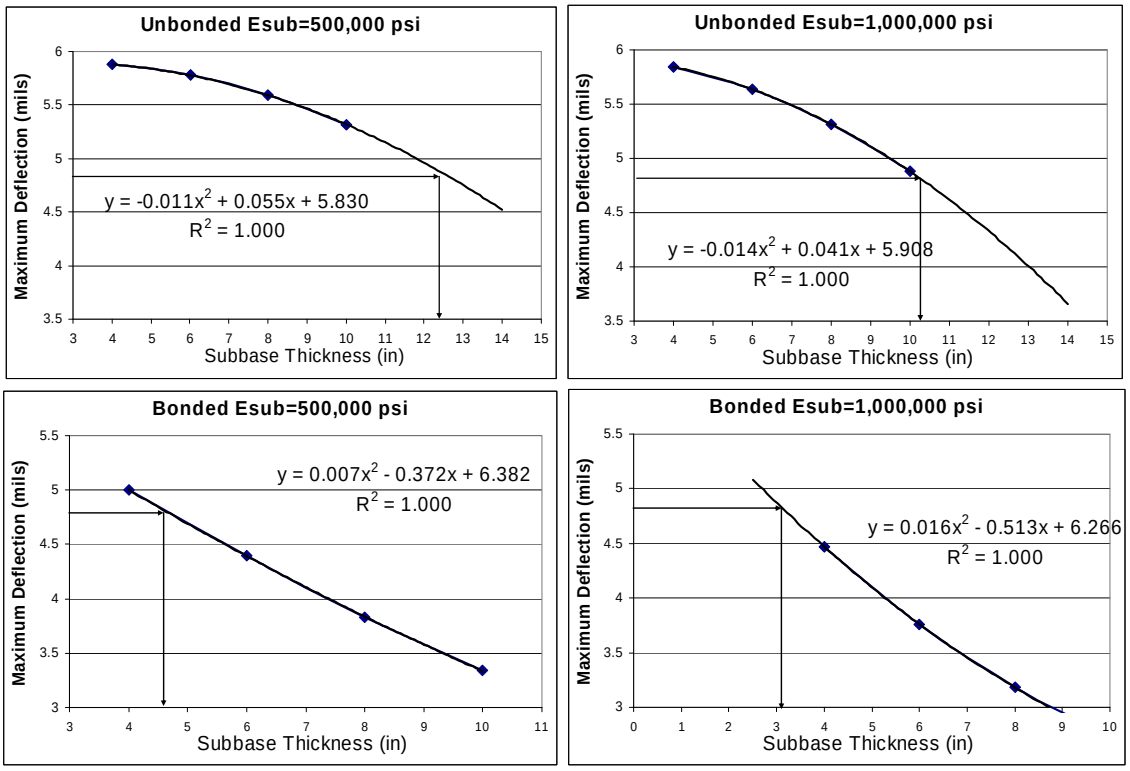

Figure 51. Subbase Thickness Corresponding to the Deflection without Subbase.

Figure 52 summarizes the results relative to a 300 psi/in of k-value support condition. When subbase thickness is 6 in with the subbase modulus of 500,000 psi, degree of bonding should be higher than the case of the subbase modulus of 1,000,000 psi to be equivalent support condition. Since degree of bonding is related to the coefficient of friction of interface, the subbase type with higher fiction would result in a higher equivalent k-value.

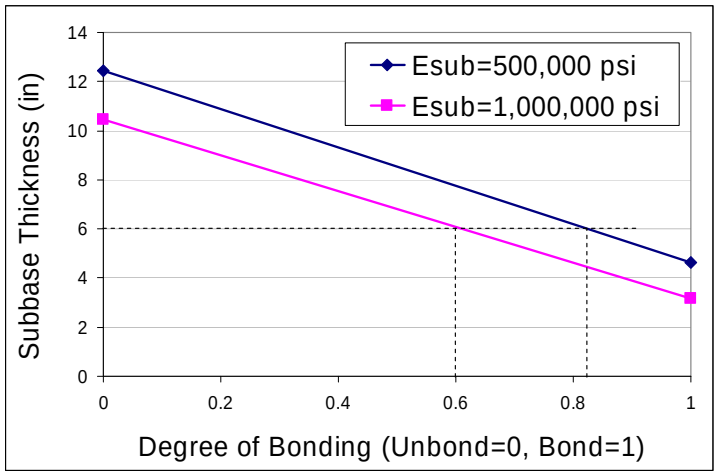

Figure 52. Subbase Thickness Design to Achieve 300 psi/in of k-value Support Condition.

K-VALUE CONSIDERATIONS RELATIVE TO CURLING AND WARPING BEHAVIOR

The stress behavior of a concrete slab due to curling is illustrated in Figure 53; it is related to the effect of the slab support immediately below the slab, particularly when a stabilized base is involved. Therefore, the joint spacing and the radius of relative stiffness is a function of the slab thickness and the effective k-value immediately below the slab. The effective k-value depends on the stiffness of the support as dictated by the subgrade k-value and the thickness and stiffness of the subbase layer supporting the concrete slab. Unfortunately, there are few established methods to determine the effective k-value other than backcalculation using the equivalent deflection approach explained earlier. Nontheless, it is well accepted that cement-treated subbases significantly increase the effective k-value over a subgrade k-value or of untreated subbases.

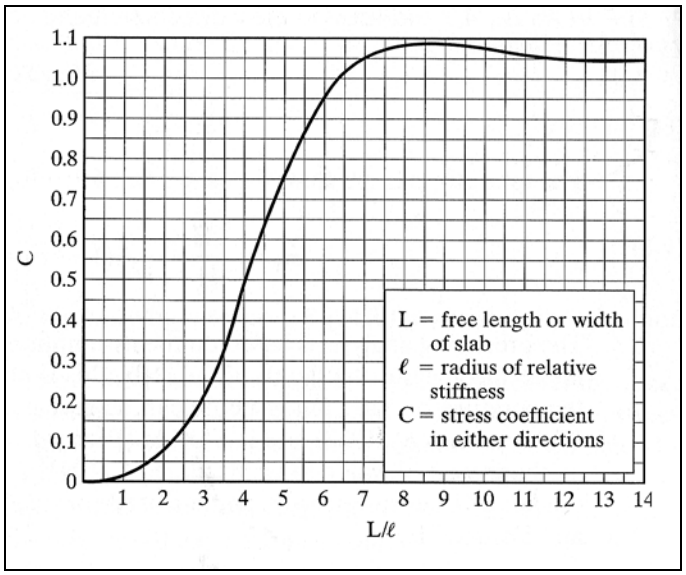

Figure 53. Stress Coefficient at the Center of Slab for the Curling Ratio L / ℓ (*16*).

The data in Table 11 is used to further elaborate on the effect of k-value on curl behavior. Assuming an equivalent k-value of 300 psi/in based on the previous analysis, daytime and nighttime situations with different temperature gradients are considered.

Table 11. Analysis Conditions.

PCC Slab Thickness	8 in	Subbase Thickness	10.44 in
E_c	4,000,000 psi	E_{sub}	1,000,000 psi
Conc. Poisson ratio	0.15	Subbase Poisson ratio	0.2
k-value	200 psi/in	Equivalent k-value	300 psi/in
Coefficient of Thermal Expansion (CoTE), α_t	4.4E-06 in/in/°F	Daytime gradient	1.65 °F/in
Slab length, L*x*	30 ft	Nighttime gradient	1.0 °F/in
Slab width, L*y*	24 ft		

Figure 54 shows the slab curl configuration and the maximum relative deflection with a concrete slab (as the difference between the corner and the point of maximum deformation). As expected, the maximum relative deflection decreases as the subbase thickness increases. A relative deflection for the day curling is 13.635 mils and night curling is -6.197 mils.

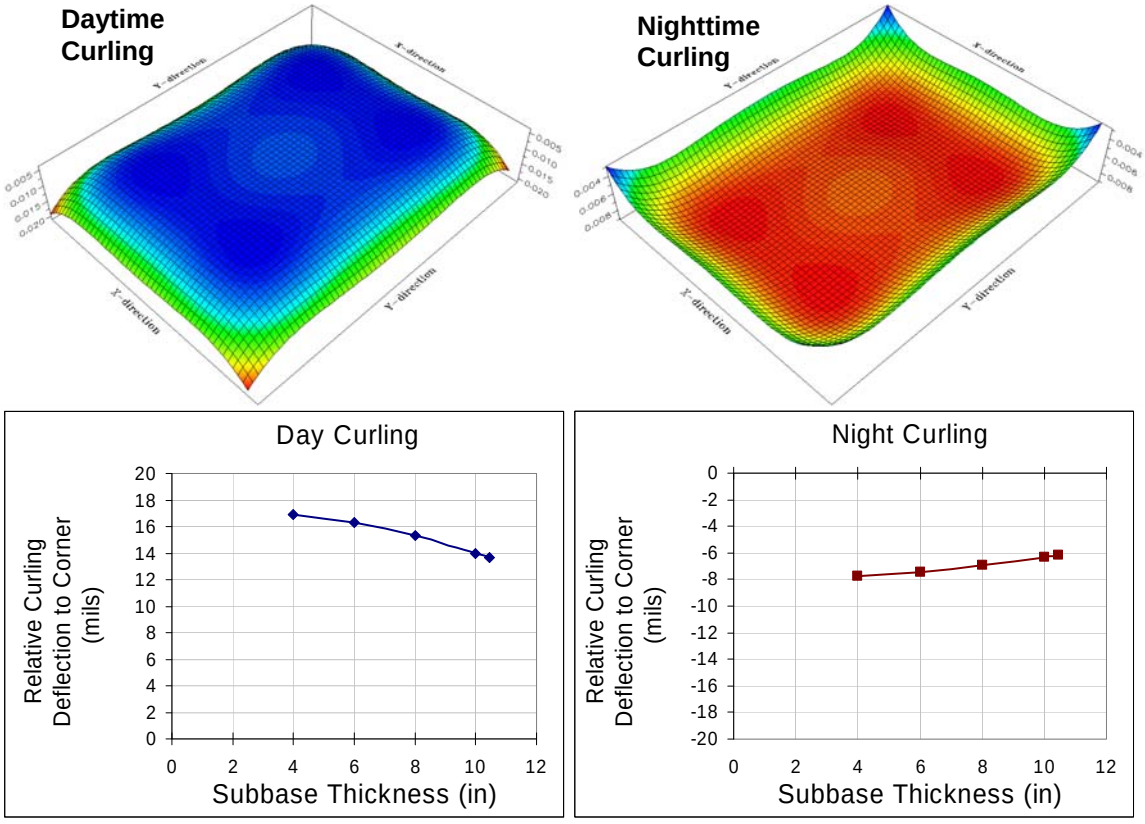

Figure 54. Curling Deflection of PCC Slab over Subbase and Subgrade (200 psi/in).

Figure 55 shows a single layer analysis for maximum relative deflection of a concrete slab over a 300 psi/in k-value subgrade. The deflections diminish exponentially with k-value and stiffer subgrade support. The regression equation in figures can be used to find the equivalent k-value by matching the deflection of a two-layer system. The analysis results clearly show the k-value for loading analysis is not the same k-value for curl analysis.

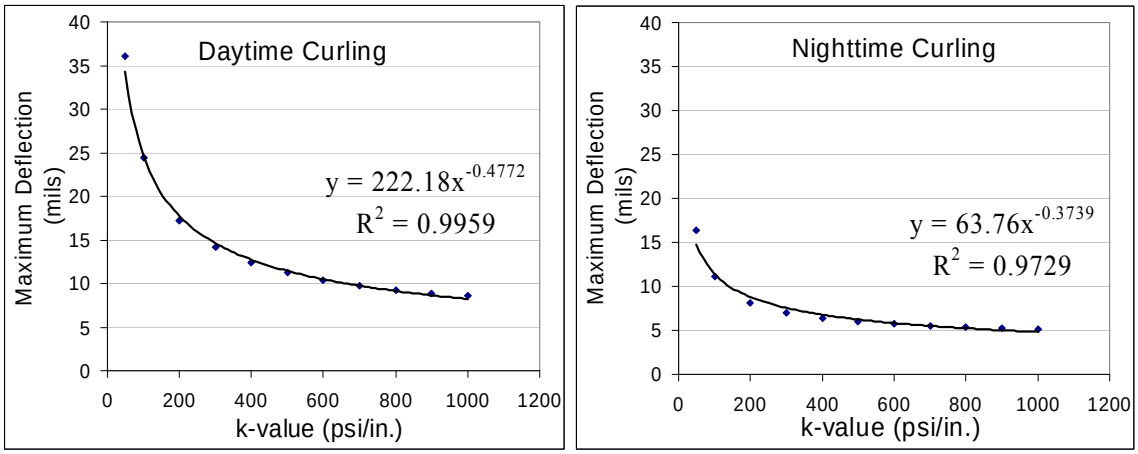

Figure 55. Curling Deflection of PCC Slab over Subgrade (No Subbase).

Table 12 and Figure 56 show the comparison of effective k-values under applied and environmentally induced loading. As shown, effective k-value derived from equivalent deflection by loading is not comparable with the k-value from curling induced deflections. In any case, the k-value should be derived by matching the deflection pattern for an actual pavement structure.

Table 12. Equivalent k-value for Various Subbase Thickness.

Subbase Thickness, in	Effective k-value by Matching of:		
	Load Induced Deflection	Curl Induced Deflection (day)	Curl Induced Deflection (night)
4	207	233	284
6	222	251	316
8	249	288	375
10	293	350	480
10.44	300	367	510

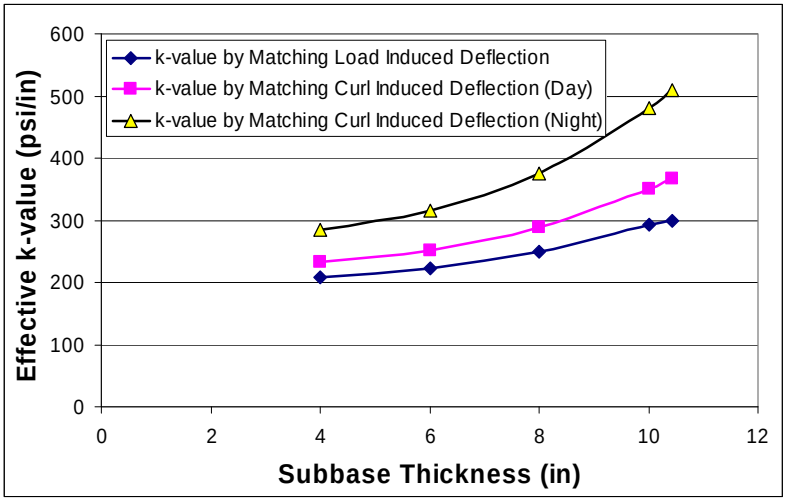

Figure 56. Equivalent k-Values by Different Analysis Methods.

FIELD EVALUATION OF SUBGRADE MODULUS OF REACTION

To evaluate the modulus of subgrade reaction under a rigid pavement system, two in-situ nondestructive tests were performed and compared. The three kinds of testing methods performed in this study were the FWD test, dynamic cone penetration test and subgrade reaction modulus test. The objectives of this testing were as follows:

1. Determine the modulus of subgrade reaction by plate load and FWD testing.
2. Examine the feasibility of k-value testing.
3. Compare results between FWD and plate load testing.
4. Assess the results of field tests.

These tests were conducted on the white topping slab located at the JJ-Pickle Research Campus at the University of Texas at Austin. The white topping slab is a full-scale (18 ft × 18 ft × 6 in) concrete slab constructed and tested during the summer of 2007. This site consists of an 8 in aggregate base, a 1.9 in asphalt surface, and a 6 in concrete slab as shown in Figure 57. The base tests were conducted on the asphalt surface as noted.

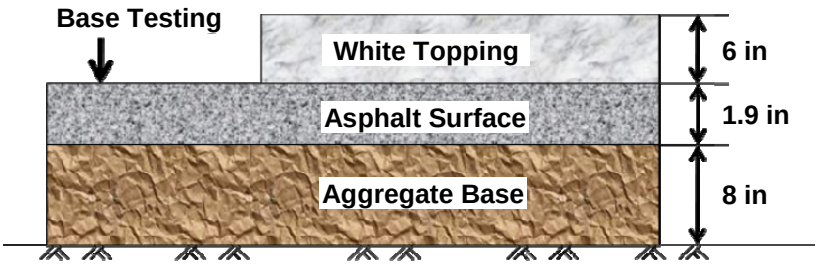

Figure 57. Composition of Test Site.

FALLING WEIGHT DEFLECTOMETER TEST

FWD test data was obtained conducted prior to slab construction to determine the elastic modulus of each layer. A total of 108 locations were selected for this data collection effort. The tests were performed at one ft grid intervals on the asphalt surface. Center plate deflections of the asphalt surface were measured under a 9000 lb load.

Figure 58 shows the FWD test result contour. Different colors mean different deflections per 1000 lb of load on the plate. Three different locations were selected to compare results. Location K8 was named as A. It is a high FWD deflection point. In other words, this is a weak support spot. Location K2 was named as B. This is a medium FWD deflection spot. Also, at this location, after removal of the asphalt surface, it was named as B-1. Finally, Location I3 was named as C. This is a low FWD deflection point and it is a strong support point. Figure 59 shows the deflections of the three reference locations along FWD sensors. Plate load testing was also conducted at these locations.

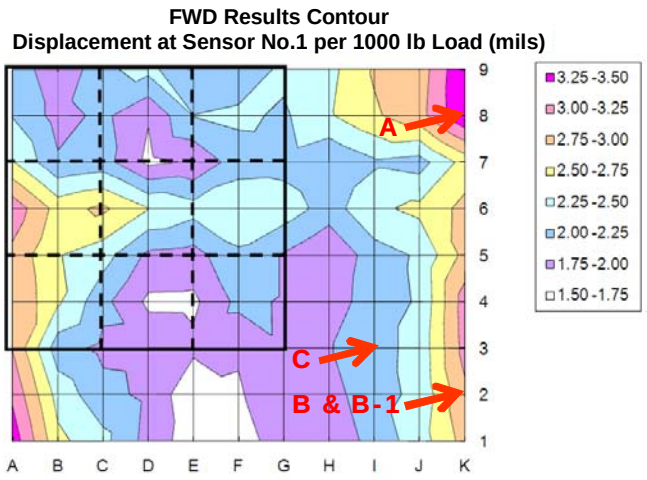

Figure 58. FWD Result Contour.

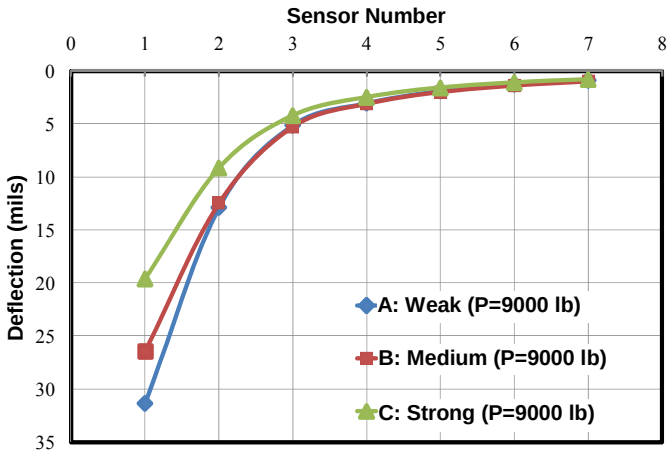

Figure 59. FWD Result along Sensors.

To determine k-value for a concrete pavement system, a backcalculation method was developed by Hall in 1991 (*17*). This method is based on deflection of an infinite slab. The dynamic k-value may be obtained from following equation.

$$k = \left(\frac{P}{8 d_0 l^2} \right)^{\left\{ 1 + \left(\frac{1}{2\pi} \right) \left[\ln\left(\frac{a}{2l} \right) + \gamma - 1.25 \right] \left(\frac{a}{l} \right)^2 \right\}} \quad \textbf{(18)}$$

where: d_0 = maximum deflection, in

P = load, lbs

γ = 0.5772 (natural logarithm of Euler's constant)

In the above equation, l represents the radius of relative stiffness, which can be calculated by the following equation:

$$l = \left[\frac{\ln\left(\frac{36 - AREA}{1812.279} \right)}{-2.559} \right]^{4.387} \quad \textbf{(19)}$$

where, the concept of *AREA* was proposed by Hoffman and Thompson in 1981 (*18*). The AREA value can be calculated by following equation:

$$AREA = 6 \times \left[1 + 2\left(\frac{d_{12}}{d_0} \right) + 2\left(\frac{d_{24}}{d_0} \right) + \left(\frac{d_{36}}{d_0} \right) \right] \quad \textbf{(20)}$$

where: d_0 maximum deflection at center of loading plate

d_i deflection at 12, 24, and 36 in from the center

Using the above equations, dynamic k-values at the three selected locations were calculated. Table 13 shows the backcalculated results.

Table 13. k-values Backcalculated from FWD Data.

Location	Dynamic k-value (psi/in)	BA (in)	Radius of Relative Stiffness (in)	Remark
A	180	13.4	10.6	High FWD Spot
B	198	14.8	11.3	Medium FWD Spot
C	256	15.2	11.5	Low FWD Spot

BASIN AREA DETERMINATION USING ELSYM5

The Elastic Layered System computer program (ELSYM5) is widely used in pavement analysis. While only applicable for analysis of the interior regions of a concrete pavement system, the various component stresses, strains, and displacements along with principal values in a three-dimensional ideal elastic-layered system can be determined by this program (*19*).

The results of field plate load test were compared with the calculated values from the ELSYM5 computer program to determine the input data. Backcalculation was carried out using the FWD test data by selecting the layer moduli to best match the deflection profile. Table 14 shows the average backcalculated elastic modulus data derived from FWD testing. Figure 60 shows input data for ELSYM5; E_{AC} is elastic modulus of the asphalt layer; E_{BS} is the elastic modulus of the aggregate base; and E_{SG} is the elastic modulus of subgrade. μ is the Poisson's ratio for each layer. In this analysis, the aggregate base was 8 in thick and the asphalt base was 2 in thick.

Table 14. Average Backcalculated Elastic Modulus from FWD Testing.

Layer	Average Elastic Modulus (psi)	Standard Deviation (psi)	Coefficient of Variance (%)
Asphalt Concrete	485,000	0.0	0.0
Aggregate Base	38,400	9.5	24.6
Subgrade	27,100	2.9	10.7

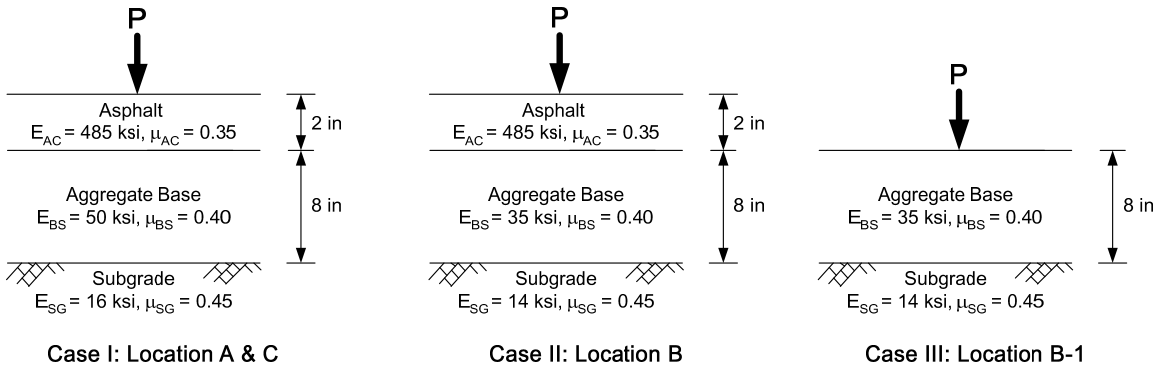

Figure 60. Input Data for ELSYM5.

As will be noted later, subgrade reaction modulus, dynamic k-value calculated by ELSYM5 is significantly smaller than the k-value determined from plate load testing but compares well with the backcalculated dynamic k-value from FWD testing. The backcalculated dynamic k-values were determined by the same process as used in the MEPDG, being based on the deflections of an equivalent pavement configuration and effective subgrade modulus that matches the deflection basin for a multilayer system.

SUBGRADE REACTION MODULUS TEST – STATIC PLATE LOAD TEST

Plate load testing using a fully loaded dump truck and load bearing plates was performed at the testing site. Plate load testing locations, as previously noted, consisted of location A as high FWD displacement point, location B as a medium FWD result point, and location C as a low FWD displacement point. Table 15 shows the selected plate load test locations, coordinates, and location descriptions.

Table 15. Plate Load Test Locations.

Location	Coordinate	9000 lb FWD Displacement at Sensor No.1 (mils.)	Expected k-value Remark
A	K8	31.4	Low modulus
B	K2	26.5	Medium modulus
C	I3	19.6	High modulus
B-1	K2	-	Test location B again; after removal of asphalt surface; repetitive testing

The static plate load test was performed based on ASTM standard, (*20*). Figure 61 shows the front view and ground view of plate load test equipment setting respectively. First of all, sand was put on the test surface to level the test location and the steel bearing plate. The steel bearing plate, which has 12 in diameter and 1 in thickness, was located on the sand. On the 12 in steel bearing plate, 9 in and 6 in diameter steel plates were stacked and centered for uniform dispersion of the load. These steel plates also have a

1 in thickness. A load cell was settled to measure load on the surface of the top steel plate. A hydraulic jack was assembled to apply the load. A fully loaded dump truck was used as reaction equipment. Gross weight of this reaction equipment was 48,000 lb.

To measure vertical displacement of the ground, two linear variable differential transformers (LVDTs) and one dial gauge were used. To install these apparatus a reference frame prevented any effect of localized subsidence due to the application of the load on the vertical measurements. To this end, a 9 ft long frame was used. Two LVDTs and one dial gauge were assembled to measure the vertical displacement. The gauges were placed on the top surface of the 12 in steel bearing plate 120 degrees apart from each other.

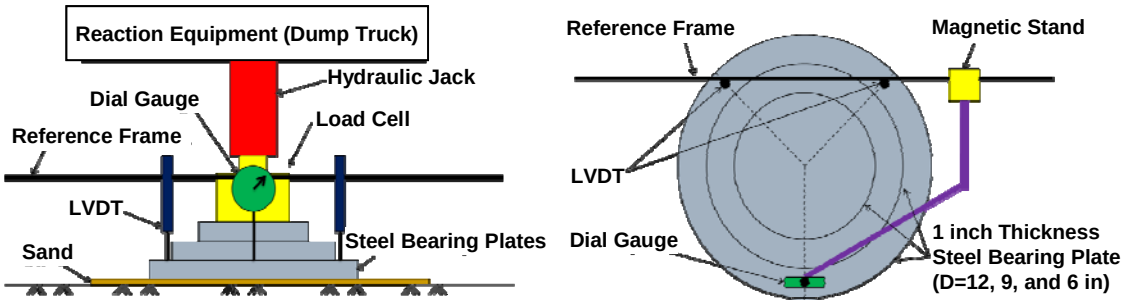

Figure 61. Plate Load Test Setting: a) Front View, and b) Ground View.

After all equipment has been properly arranged, initial loading was applied for seating purposes. The preload was released after the LVDTs were stabilized. After stabilizing, load was applied again at a moderately rapid rate in uniform 0.005 in increments. Each increment of load was applied at a rate of deflection not more than 0.001 in/min. Load and deflection readings were recorded for each load increment. This process continued until the total deflection was more than 0.05 in For all cases, more than 6 load-deflection points were obtained. The modulus of subgrade reaction was calculated at a 0.05 in deflection as is the TxDOT practice (*21*). Figure 62 shows the plate load field test.

Figure 62. Plate Load Field Test.

Figure 63 shows the plate load test result at location C. Figure 64 shows the plate load test result at three selected locations. From these load-deflection curves, k-value can be calculated by the following equation:

$$k = \frac{p}{\Delta} = \frac{p_{\Delta=0.05}}{0.05} \quad \textbf{(21)}$$

where, P is the loading pressure in psi and the calculated k-value has a units of pound per square inch per inch (psi/in). The k-values calculated by the nonrepetitive plate load test are shown in Table 16. Composite k-values ranging from 1340 to1840 psi/in were obtained. The largest value, 1840 psi/in was produced at location C. This location is a low FWD deflection area. Therefore, it is clear that FWD test and plate load tests show similar results at the location C. However, the k-value from location A and B are almost similar, although the FWD result of location A was much higher than that of location B. Also, the repetitive plate load test was performed at location B-1 with results shown in Figure 65.

This form of testing is clearly compromised by the layering above the subgrade level. Plate load tests are, of course, normally run on the subgrade, but tests on location A, B, and C were run on top of the AC surface layer over an aggregate subbase. Additionally, the layer stiffness, interlayer friction, and bonding between the layers resulted in excessively high k-values.

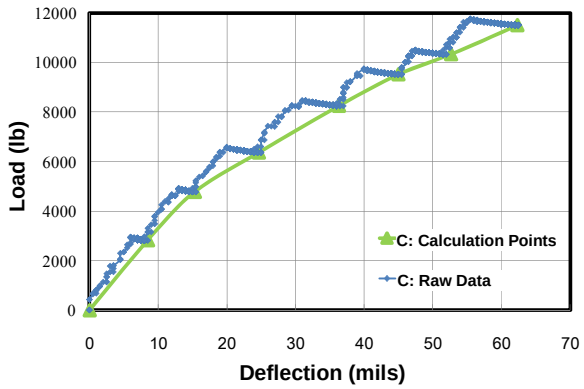

Figure 63. Plate Load Test Result of Location C.

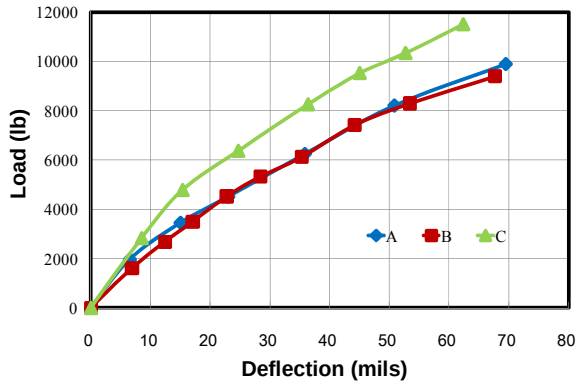

Figure 64. Plate Load Test Result of Three Locations.

Table 16. k-values by Plate Load Test.

Location	k-value (psi/in)	Remark
A	1360	High FWD Spot
B	1340	Medium FWD Spot
C	1840	Low FWD Spot
B-1	840	After removal of asphalt surface at Location B

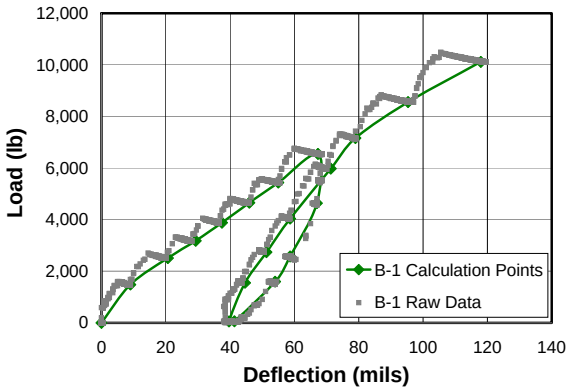

Figure 65. Repetitive Plate Load Test Result at Location B-1.

COMPARISON OF RESULTS AND DISCUSSIONS

Table 17 shows the backcalculated elastic moduli and dynamic k-values resulting from the analysis of the FWD and the elastic layer basin data. The results are similar indicating the advantage of using the basin area concept. Clearly, the static plate loading test is only appropriate for low cohesive materials where interlayer friction and bonding is a minimum.

Table 17. Comparison Among FWD, DCP, Plate Load Test, and ELSYM5.

Location	Elastic Modulus (ksi)		Subgrade Dynamic k-value (psi/in)	
	FWD Deflection Data		Using FWD BA Data	Using ELSYM5 BA Data
	E_{base}	$E_{subgrade}$		
A	50	16	180	226
B	35	14	198	188
C	50	16	256	226
B-1	35	14	-	163

It is pointed out that the theoretical difference between a k-subgrade model and an elastic foundation model is manifest in the deformation along plate edge (Figure 66). A k-value is simply a linear spring constant consisting of units of force/unit area/unit

length (i.e., psi/in) where springs are individually grouped in parallel as a series of springs under the slab that are void of any type of shearing behavior within the supporting medium which has been one of the primary shortcomings of this type of model. A k-value foundation model characteristically displays a discontinuity in the pattern of the subgrade deformation at the edge of the slab. If the soil model included a shear strength term, the pattern of the displacement would be more gradual in nature at the plate edge as would be displayed by elastic solid behavior.

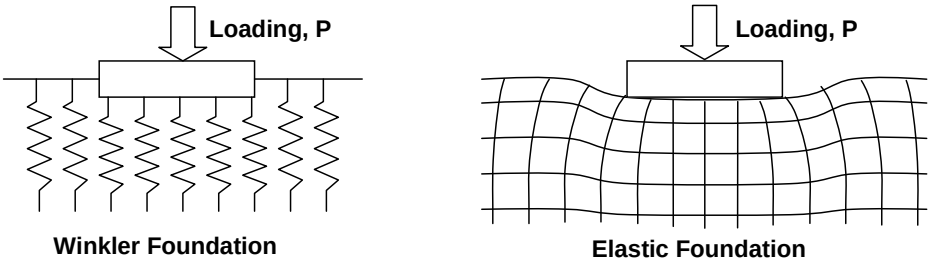

Figure 66. Subgrade Model and Loading Behavior.

CHAPTER 9
SUMMARY AND CONCLUSIONS

The objectives of the field investigation were to identify the factors associated with the erosion process. To this end, sections of US 75, US 81/287, FM 364, IH 10, and IH 635 were sampled and investigated using a number of techniques including visual survey, nondestructive testing using FWD, and GPR as well as DCP testing and coring.

Generally, untreated flexible base has not performed well particularly over moisture sensitive subgrades while most CSB have performed well particularly when used with an AC interlayer due to high resistance to erosion.

Untreated aggregate base on US 75 in the Sherman area showed poor performance, possibly due to poor subgrade drainage and poor support. The modulus of the base in the patched area was about twice the base modulus of the unrepaired sections.

An AC base on a lime-treated subgrade on US 81/287 in Wise County has performed reasonably well except in areas where the subbase and subgrade was eroded. The bond condition between the PCC and AC base layer was generally good but erosion between the slab and the AC layer and between the AC layer and the lime-treated subgrade diminished the structural integrity of the pavement.

The cement stabilized oyster shell base on FM 364 in the Beaumont area showed erosion at the interface with the PCC near the joint but no erosion was noted away from the joint as indicated by the good contact between the concrete slab and the base.

Distressed areas on the frontage road along IH 10 in Beaumont consisted of severe map cracking, spalling, and pumping due to placement of a CRC pavement over a soft silty and sandy subgrade. Some patched areas had settled and experienced corner breaks due to low LTE and poor support. Most of the damage appeared to be due to a weak subgrade.

The key distress types of CRC pavement over CSB on IH 635 in the Dallas area were the condition of the full-depth patches and the widened longitudinal joints, although the overall condition of the pavement appeared to be very good. The patches in the pavement were mostly likely repairs of punchout distress that are possibly a result of erosion and loss of support immediately below the slab.

The induced shear stress along the interface between concrete slab and base layer plays a major role in the erosion process. As the stiffness of the joint or crack decreases, the slab shear stress increases under the applied loading generating fines along the slab-subbase interface which are susceptible to dislocation under pressurized water movement via pumping through joint or crack to the pavement surface. Pumping results in a void under the slab and leads to a loss of joint stiffness.

The erosion of material beneath the slab is an important performance-related factor that needs to be addressed in the selection of base materials as part of the design process for concrete pavements. In this regard, general design factors such as concrete slab stiffness, traffic, environmental factors and strength and abrasion resistance (or shear strength) of the base and subgrade materials should be considered relative to erodibility. Moreover, drainage and layer frictional conditions should be considered in the design process in order to consider the full extent of erosion damage. As background, past and current methods (including models) relative to erosion were reviewed.

The presence of water, the erodibility of a subbase material, the rate of voiding, the amount of deflection, and the number of loads are factors that influence erosion but current design procedures scarcely address these factors. Many erosion tests were developed in the 1970s and 1980s using various testing devices but none of those tests have been interpretable relative to field performance. Erosion test methods were reviewed and evaluated relative to their utility to characterize subbase and subgrade materials for erosion resistance relative to performance.

A list of alternative subbase types and materials were assembled based on the evaluation of field performance and other functional factors. Accordingly, the experience with the use of cement-treated base had been good and recyclable materials (recycled asphalt and recycled concrete) show promise economically. Testing of selected materials is currently underway and results to date are summarized as well as a new test procedure to evaluate erosion.

The effect of a stabilized layer in a rigid pavement system was characterized relative to bending and deflection behavior using the ISLAB 2000 program. The relationship between the modulus of subgrade reaction and the elastic modulus was reviewed. The effective k-value from equivalent deflection is different for load and

curling slab behavior. The elastic moduli and dynamic k-values from the backcalculation of FWD and ELSYM5 are comparable; however, the interpretation of k-value from plate load testing is susceptible to edge boundary and frictional condition. Nonetheless, a methodology shows how to consistently and realistically characterize CSB layers with respect to a specific level of support.

Clearly, the advantage of a design framework is to relate the characteristics of the base to performance in terms of the base thickness, stiffness, coefficient of friction, and strength and better understanding the use of subbase materials in terms of their effect on pavement performance. The tools to advance pavement design to the next level with respect to subbase performance are readily available and can be assembled from the test results generated in this research program

REFERENCES

1. Zollinger, C.J., D.G. Zollinger, D.N. Little, and A. Godiwalla. "Innovative Approach to Pavement Rehabilitation Analysis and Design of Runway (R/W) 15L-33R at George Bush Intercontinental Airport (IAH) in Houston, TX," Proceedings, 8th International Conference on Concrete Pavements, Colorado Springs, Colorado, August 15-18, 2005, Vol. 3, pp.1101-1119.

2. Webster, S.L., R.H. Grau, and T.P. Williams, "Description and Application of the Dual Mass Dynamic Cone Penetrometer. Instruction Report GL-93-3," Department of Army, Waterways Experiment Station, Corps of Engineers, Vicksburg, Mississippi, 1992, pp. 50.

3. "Guide for Design of Pavement Structures," American Association of State Highway and Transportation Officials, Washington, D.C., 1986.

4. Van Wijk, A.J., "Rigid Pavement Pumping: (1) Subbase Erosion and (2) Economic Modeling," Joint Highway Research Project File 5-10. School of Civil Engineering, Purdue University, West Lafayette, Indiana., May 16, 1985.

5. Phu, N.C., and M. Ray, "The Erodibility of Concrete Pavement Subbase and Improved Subgrade Materials," Bulletin de Liaison des Laboratoires des Ponts et Chaussees, France, Special Issue 8, July 1979, pp. 32-45.

6. Huang, Y.H., "Pavement Analysis and Design," 2nd Edition, Pearson Prentice Hall, Upper Saddle River, New Jersey, 2004.

7. "Guide for Mechanistic-Empirical Design of New and Rehabilitated Pavement Structures: Final Document Appendix JJ: Transverse Joint Faulting Model," National Cooperative Highway Research Program, http://www.trb.org/mepdg/guide.htm, updated: August 2003, accessed: October 1, 2008.

8. Jeong, J,. and D. Zollinger, "Characterization of Stiffness Parameters in Design of Continuously Reinforced and Jointed Pavements," Transportation Research Record 1778, TRB, National Research Council, Washington, D.C., 2001, pp. 54-63

9. de Beer, M., "Aspects of the Erodibility of Lightly Cementitious Materials," Research Report DPVT 39, Roads and Transport Technology, Council for Scientific and Industrial Research, Pretoria, South Africa.

10. "Pavement – Soil Cement," Portland Cement Association, Skokie, Illinois http://www.cement.org/pavements/pv_sc.asp, updated: 2008, accessed: October 1, 2008.

11. "Reclaimed Asphalt Pavement - User Guideline—Asphalt Concrete," Turner-Fairbank Highway Research Center, McLean, Virginia, http://www.tfhrc.gov/hnr20/recycle/waste/rap131.htm, accessed: October 1, 2008.

12. Guthrie, W.S., S. Sebesta, and T.Scullion, "Selecting Optimum Cement Contents for Stabilized Aggregate Base Materials," Report 4920-2. Texas Transportation Institute, Texas A&M University System, College Station, Texas, February, 2002.

13. Lim, S., D. Kestner, D.G. Zollinger, and D.W. Fowler, "Characterization of Crushed Concrete Materials for Paving and Non-paving Applications," Report 4954-1. Texas Transportation Institute, Texas A&M University System, College Station, Texas, January 2003.

14. "Summary of Texas Recycled Concrete Aggregate Review," United States Department of Transportation—Federal Highway Administration, http://www.fhwa.dot.gov/pavement/recycling/rcatx.cfm, modified: July 18, 2006, accessed: October 1, 2008.

15. "Guide for Mechanistic-Empirical Design of New and Rehabilitated Pavement Structures: Final Document Part 3 Design Analysis, Chapter 4 Design of New and Reconstructed Rigid Pavements," National Cooperative Highway Research Program, http://www.trb.org/mepdg/guide.htm, updated: March 2004, accessed: October 1, 2008.

16. Bradbury, R.D. "Reinforced Concrete Pavement," Wire Reinforcement Institute, Washington, D.C., 1938.

17. Hall, K.T., "Performance, Evaluation, and Rehabilitation of Asphalt-Overlaid Concrete Pavements." Ph.D. Thesis, University of Illinois at Urbana-Champaign, Urbana-Champaign, Illinois, 1991.

18. Hoffman, M.S. and M.R. Thompson, "Mechanistic Interpretation of Nondestructive Pavement Testing Deflections," Transportation Engineering Series No. 32, Illinois Cooperative Highway and Transportation Research Series No. 190, University of Illinois at Urbana-Champaign, Urbana-Champaign, Illinois, 1981.

19. Hicks, R.G., "Use of Layered Theory in the Design and Evaluation of Pavement System," Research Report FHWA-AK-RD-83-8, Alaska DOTPF Research Section, 1982.

20. ASTM D 1196, "Standard Test Method for Nonrepetitive Static Plate Load Tests of Soils and Flexible Pavement Components, for Use in Evaluation and Design of Airport and Highway Pavements" ASTM International, West Conshohoken, Pennsylvania, 2004, 3 pp.

21. Tex-125-E, "Determining Modulus of Sub-grade Reaction (k-Value)" Texas Department of Transportation, Austin, Texas, 1999.